Allele-specific silencing as treatment for gene duplication disorders: proof-of-principle in autosomal dominant leukodystrophy

OXFORD UNIVERSITY PRESS | Brain

Allele-specific silencing as treatment for gene duplication disorders: a proof-of-principle in Autosomal Dominant LeukoDystrophy

Journal:	*Brain*
Manuscript ID	BRAIN-2018-00582.R1
Manuscript Type:	Original Article
Date Submitted by the Author:	n/a
Complete List of Authors:	Giorgio, Elisa; University of Torino, Department of Medical Sciences Lorenzati, Martina; University of Torino, Department of Neurosciences Rivetti di Val di Cervo, Pia; Universita degli Studi di Milano, Department of Biosciences Brussino, Alessandro; University of Torino, Department of Medical Sciences Cernigoj, Manuel; Universita degli Studi di Milano, Department of Biosciences Della Sala, Edoardo; University of Torino, Department of Medical Sciences Bartoletti Stella, Anna; Ospedale Bellaria Carlo Alberto Pizzardi, IRCCS Institute of Neurological Sciences Ferrero, Marta; University of Torino, Department of Medical Sciences Caiazzo, Massimiliano; Universiteit Utrecht, Department of Pharmaceutics; Universita degli Studi di Napoli Federico II, Department of Molecular Medicine and Medical Biotechnology Capellari, Sabina; Ospedale Bellaria Carlo Alberto Pizzardi, IRCCS Institute of Neurological Sciences; University of Bologna, Department of Biomedical and Neuromotor Sciences Cortelli, Pietro; Ospedale Bellaria Carlo Alberto Pizzardi, IRCCS Institute of Neurological Sciences; University of Bologna, Department of Biomedical and Neuromotor Sciences Conti, Luciano; University of Trento, Centre for Integrative Biology (CIBIO), Laboratory of Computational Oncology Cattaneo, Elena; University of Milano, Dept of Pharmacological Sciences Buffo, Annalisa; University of Turin, Department of Neuroscience, Neuroscience Institute Cavalieri Ottolenghi Brusco, Alfredo; University of Torino, Department of Medical Sciences
Subject category:	Genetics
To search keyword list, use whole or part words followed by an *:	Gene therapy < GENETICS, Leukodystrophy < MULTIPLE SCLEROSIS AND NEUROINFLAMMATION, Demyelination < MULTIPLE SCLEROSIS AND NEUROINFLAMMATION, Myelin < NEUROMUSCULAR DISEASES, Oligodendrocyte < MULTIPLE SCLEROSIS AND NEUROINFLAMMATION

Allele-specific silencing as treatment for gene duplication disorders: a proof-of-principle in Autosomal Dominant LeukoDystrophy.

Elisa Giorgio[1], Martina Lorenzati[2], Pia Rivetti di Val Cervo[3], Alessandro Brussino[1], Manuel Cernigoj[3], Edoardo Della Sala[1], Anna Bartoletti Stella[4], Marta Ferrero[1], Massimiliano Caiazzo[5,6], Sabina Capellari[4,7], Pietro Cortelli[4,7], Luciano Conti[8], Elena Cattaneo[3,9], Annalisa Buffo[2], Alfredo Brusco[1,10]

[1] University of Torino, Department of Medical Sciences, 10126, Torino, Italy.

[2] University of Torino, Department of Neuroscience Rita Levi Montalcini and Neuroscience Institute Cavalieri Ottolenghi (NICO), Orbassano, 10043, Torino, Italy.

[3] University of Milan, Department of Biosciences, Laboratory of Stem Cell Biology and Pharmacology of Neurodegenerative Diseases, 20122 Milan, Italy

[4] IRCCS Istituto delle Scienze Neurologiche di Bologna, Bellaria Hospital, 40139, Bologna, Italy.

[5] Department of Pharmaceutics, Utrecht Institute for Pharmaceutical Sciences (UIPS), Utrecht University, Universiteitsweg 99, 3584, CG, Utrecht, The Netherlands.

[6] Department of Molecular Medicine and Medical Biotechnology, University of Naples "Federico II", 80131, Naples, Italy.

[7] University of Bologna, Department of Biomedical and Neuromotor Sciences, 40123, Bologna, Italy

[8] University of Trento, Centre for Integrative Biology (CIBIO), Laboratory of Computational Oncology, 38123, Trento, Italy.

[9] National Institute of Molecular Genetics (INGM) Romeo and Enrica Invernizzi, 20122, Milano, Italy

[10] Città della Salute e della Scienza University Hospital, Medical Genetics Unit, 10126, Torino, Italy.

Corresponding author: Alfredo Brusco, University of Torino, Department of Medical Sciences, via Santena 19, 10126, Torino, Italy. Fax +390112365926; e-mail: alfredo.brusco@unito.it

Short title: Allele specific silencing in ADLD

Keywords: ADLD; LMNB1, leukodystrophy, therapy, antisense oligonucleotide, siRNA

Conflict of interest: Alfredo Brusco and Elisa Giorgio are authors of the patent n. 102017000121288, concerning the ASP-siRNA sequences.

ABSTRACT

Allele-SPecific silencing by RNA Interference (ASP-siRNA) holds promise as a therapeutic strategy for downregulating a single mutant allele with minimal suppression of the corresponding wild-type allele. This approach has been effectively used to target autosomal dominant mutations and single nucleotide polymorphisms (SNPs) linked with aberrantly expanded trinucleotide repeats. Here, we propose ASP-siRNA as a preferable choice to target duplicated disease genes, avoiding potentially harmful excessive downregulation. As a proof-of-concept, we studied Autosomal Dominant adult-onset demyelinating LeukoDystrophy (ADLD) due to Lamin B1 (*LMNB1*) duplication, a hereditary, progressive and fatal disorder affecting myelin in the central nervous system. Using a reporter system, we screened the most efficient ASP-siRNAs preferentially targeting one of the alleles at rs1051644 (average MAF: 0.45) located in the 3'-UTR of the gene. We identified four siRNAs with a high efficacy and allele-specificity, which were tested in ADLD patient-derived fibroblasts. Three of the siRNAs were highly selective for the target allele and restored both LMNB1 mRNA and protein levels close to control levels. Further, siRNA treatment abrogates the ADLD-specific phenotypes in fibroblasts and in two disease-relevant cellular models: murine oligodendrocytes overexpressing human Lamin B1, and neurons directly reprogrammed from patients' fibroblasts.

In conclusion, we demonstrated that ASP-silencing by RNAi is a suitable and promising therapeutic option for ADLD. Moreover, our results have a broad translational value extending to several pathological conditions linked to gene-gain in copy number variations.

INTRODUCTION

Autosomal Dominant adult-onset demyelinating LeukoDystrophy (ADLD, OMIM#169500) (Eldridge *et al.*, 1984) is a slowly progressive disease which occurs in the 4th-5th decade of life with autonomic symptoms, which can precede cerebellar and pyramidal abnormalities by several years. Loss of fine motor control and gait disturbance appear later and culminate in slowly progressive spastic tetraparesis, ataxia, and incontinence (Quattrocolo *et al.*, 1997; Coffeen *et al.*, 2000; Nahhas, 2016). Only symptomatic and palliative treatments are presently available. ADLD is caused by excessive Lamin B1 (LMNB1) production due to gene duplication (Padiath *et al.*, 2006; Giorgio *et al.*, 2013) or to alteration of the Lamin B1 regulatory landscape (Giorgio *et al.*, 2015)(Nmezi *et al.,* 2019).

At the cellular level, LMNB1 regulates nuclear mechanics and integrity (Ferrera *et al.*, 2014), interacts with chromatin determining chromosome segregation (Guelen *et al.*, 2008), and regulates gene expression through mRNA synthesis (Tang *et al.*, 2008) and splicing (Camps *et al.*, 2014; Bartoletti-Stella *et al.*, 2015). The pathogenic mechanisms underlying ADLD have only begun to be explored and directly involve *LMNB1* overexpression (Heng *et al.*, 2013; Bartoletti-Stella *et al.*, 2015; Rolyan *et al.*, 2015; Giacomini *et al.*, 2016). It stands to reason that genetic modulation of Lamin B1 mRNA/protein represents a promising strategy for treating ADLD (Lin and Fu, 2009).

In recent years, the use of synthetic small interfering RNAs (siRNAs) has become a popular choice for the development of gene-silencing based therapies (Bumcrot *et al.*, 2006; Dykxhoorn and Lieberman, 2006; Levin, 2019). A handful of siRNAs have recently entered clinical trials, and others are clinically approved or in preclinical development for diseases such as autosomal dominant transthyretin amyloidosis, respiratory syncytial virus infection, solid tumors, age-related macular degeneration, diabetic macular edema, congenital pachyonychia, and hemophilia (Dykxhoorn and Lieberman, 2006; de Fougerolles *et al.*, 2007; Haussecker, 2008; Nguyen *et al.*, 2008; Smith *et al.*, 2008; Whitehead *et al.*, 2009; Davis *et al.*, 2010; DeVincenzo *et al.*, 2010;

Coelho *et al.*, 2013)(see clinicaltrials.gov).

Other than a complete suppression of the target gene, Allele-SPecific silencing by RNA interference (ASP-RNAi) has been proposed as a variant gene-silencing strategy that allows downregulation of the mutant allele with minimal suppression of the corresponding wild-type (WT) allele. ASP-siRNAi has been used to target gain-of-function autosomal dominant mutations (Miller *et al.*, 2004; Liao *et al.*, 2011; Loy *et al.*, 2012; Takahashi *et al.*, 2012; Allen *et al.*, 2013; Jiang *et al.*, 2013) and single nucleotide polymorphisms (SNPs) in *cis* with an aberrant transcript, such as in diseases with expanded polyglutamine encoding CAG-repeats (SCA1, SCA3, SCA7, and Huntington's disease) (Miller *et al.*, 2003; Alves *et al.*, 2008; Scholefield *et al.*, 2009; Takahashi *et al.*, 2010; Nobrega *et al.*, 2013; Nobrega *et al.*, 2014). It stands to reason that gene-silencing approaches represent the paramount therapeutic strategy also for genetic diseases associated with gene duplication. However, a major drawback is dysregulation and excessive transcript reduction of the target, which may lead to pathogenic consequences. This concern is due to the fact that dosage-sensitive genes often cause pathological phenotypes either in excess or defect (Antonarakis, 2017; Deshpande and Weiss, 2018). Two instructive examples are the 16p11.2-related microcephaly / macrocephaly caused by duplications or deletions encompassing the *KCTD13* gene (Jacquemont *et al.*, 2011), and the Charcot-Marie-Tooth disease, type 1A (CMT1A) / Hereditary Neuropathy with liability to Pressure Palsies (HNPP), associated with peripheral myelin protein 22 (*PMP22*) duplication or deletion, respectively (van Paassen *et al.*, 2014).

In this study, we investigated the therapeutic potential of ASP-RNAi for gene duplication disorders, having a proof-of-principle in ADLD.

Compared to other antisense strategies, this approach allows avoiding potentially harmful excessive downregulation of the target gene. This latter point seems to be relevant for *LMNB1*, where excessive silencing may have deleterious effects, as shown in cellular and mouse models (Liu *et al.*, 2000; Harborth *et al.*, 2001; Vergnes *et al.*, 2004; Ji *et al.*, 2007; Coffinier *et al.*, 2010; Coffinier *et*

al., 2011; Bartoletti-Stella *et al.*, 2015; Giacomini *et al.*, 2016).

Since ADLD patients have three, equally expressed, *LMNB1* alleles (Giorgio *et al.*, 2013), we have chosen to target the non-duplicated allele of the *LMNB1* gene by ASP-siRNAs, with the aim of reducing expression close to wild-type level (Fig. 1). To discriminate the three *LMNB1* alleles in ADLD patients, we have exploited the SNP rs1051644, located in the 3'-UTR of the gene. This polymorphism has an allele frequency ranging from 0.3 (African), 0.46 (European) to 0.53 (East Asian) (http://gnomad.broadinstitute.org)(Lek *et al.*, 2016); among our ten ADLD patients, eight carried one allele (non-duplicated allele) different from the other two (duplicated allele) (possible genotypes: C-C-T or T-T-C).

To the best of our knowledge, this is the first application of ASP-siRNAi strategy to diseases caused by gene duplications, opening new therapeutic opportunities for several pathological conditions linked to gene copy number variations.

MATERIALS AND METHODS

Plasmid vectors are described in supplementary materials.

Cell lines and cell culture.

Fibroblast cell lines were obtained from four ADLD patients [IT1, IT2, IT3, and BR1, see (Giorgio *et al.*, 2013)] and three age-matched controls. IT1, IT2, and IT3 carry the "C" allele of the targeted SNP on the duplicated *LMNB1* copy (hence named "dupC"), whereas in BR1 patient the "T" allele is duplicated (hence named "dupT").

The HEK293T cells and patients' derived fibroblasts were cultured in Dulbecco's modified Eagle's Medium (DMEM; Thermo Fisher Scientific, Waltham, MA) with the addition of 10% fetal bovine serum (FBS; Thermo Fisher Scientific). All cultures were incubated at 37°C in the presence of 5% CO_2. For direct-reprogramming experiments, human primary fibroblasts from healthy and ADLD

donors were cultured in DMEM supplemented with 10% FBS, 0.5% Pen-Strep, 2mM Glutamine, 1mM Sodium Pyruvate and 1% Non-Essential Aminoacids (Thermo Fisher Scientific).

Primary oligodendrocyte precursors were isolated by shaking method from mixed glial cultures obtained from P0-2 Sprague-Dawley rat cortex, as described in (Boda *et al.*, 2015). OPCs were plated at 20,000 cells/cm^2 onto poly-D-lysine (1 mg/mL, Sigma-Aldrich, Milan, Italy) coated Thermo Scientific Nunc Lab-Tek II chambered Coverglass, and cultured in Neurobasal with 1X B27 (Invitrogen, Milan, Italy), 2 mM L-glutamine, 10 ng/mL human platelet derived growth factor (PDGF)-BB and 10 ng/ mL human basic fibroblast growth factor (bFGF) (Miltenyi Biotec, Calderara di Reno, Italy).

Design of siRNAs and generation of shRNA Recombinant Lentivirus particles.

We designed a siRNA library with a 19+2 bp geometry, as described in (Schwarz *et al.*, 2006), targeting the "C" or the "T" alleles of the rs1051644 SNP. Because bioinformatics cannot optimally predict the best allele-specific siRNAs, all 19 possible siRNAs were considered (Suppl. table 2). A siRNA targeting the *Renilla Luciferase* gene (si*Ren*, C+) and a nonspecific siRNA (scramble) were used as controls in the experiments. All siRNAs were synthesized with a dTdT 3'-end tail by Eurofins Genomics (Ebersberg, Germany).

The most efficient ASP-siRNA (SNP position 4) targeting the T allele was converted to generate a mCHERRY-tagged short-hairpin RNA expression vector and cloned into Recombinant Lentivirus particles (LV-ASP-T4 shRNA; pLV[shRNA]-mCherry:T2A:Puro-U6; viral titer 1.62x10^9 TU/mL; outsourced to Vector Builder). As negative control, we used a commercial GFP-tagged scramble shRNA control lentivirus (scramble shRNA; viral titer 9.59x10^8 TU/mL, VB151023-10034; Vector Builder; LV-). The lentiviral particles produced were resuspended in Hank's Balanced Salt Solution (HBSS) buffer. Viral stocks were stored at -80°C until use. The virus was subsequently titered in primary cultures of rat oligodendrocyte progenitor cells (OPCs, see below) by serial dilutions. Five

days post-infection, cells were collected, and the rate of transduction evaluated by fluorescent microscopy.

Dual Luciferase Reporter Assay.

HEK293T cells were seeded at a concentration of $2.5x10^4$ cells/well in a 96-well plate and incubated for 24 hours in DMEM supplemented with 5% FCS without antibiotics. Twenty nanograms of the psiCHEK-LMNB1-3'UTR-C or the psiCHEK-LMNB1-3'UTR-T vectors were co-transfected with each siRNAs at two different concentrations (12.5 nM or 30 nM) using Lipofectamine 2000, following the manufacturer's protocol (Thermo Fisher Scientific). Chemiluminescence was measured at 48 hours post-transfection using the Dual-Luciferase® Reporter Assay System (Promega) on an analytical Glomax 20/20 luminometer (Promega). All 19 SNP-specific siRNAs, as well as si*Ren* and scramble siRNA were tested, evaluating their ability to silence the targeted psiCHEK-LMNB1-3'UTR plasmid. For each assay, we performed at least three independent technical replicas.

Validation of allele-specific siRNAs in ADLD fibroblasts.

ADLD and control fibroblasts were seeded at a concentration of $1.5x10^5$ cells/well in a 6-well plate and incubated for 24 hours in DMEM supplemented with 5% FCS without antibiotics. Cells were transfected with allele-specific siRNAs, a non-allele-specific LMNB1 siRNA (C+) and a scramble siRNA (AM 4620, Thermo Fisher Scientific) at two concentrations (40 nM and 100 nM) using Lipofectamine 2000 (Thermo Fisher Scientific). Cells were harvested at forty-eight hours post transfection and split to extract RNA and proteins.

To evaluate the ability of siRNAs to rescue ADLD-specific cellular phenotypes, ADLD and control fibroblasts were transfected using Lipofectamine 2000 (Thermo Fisher) at T0 and T72 hours with 100 nM of the allele-specific siRNAs, a non-allele-specific *LMNB1* siRNA (C+) and a scramble

siRNA (AM 4620, Thermo Fisher Scientific). Since the rescue of the reported cellular phenotypes is subsequent to LMNB1 modulation, we harvested cells at 120 hours post transfection. For each siRNA, at least three independent experiments were performed. Due to technical reasons, we were only able to test ASP-siRNA in BR1 cells.

Direct reprogramming of ADLD and control human fibroblasts in neurons.

Viral production and titration. HEK293NT cells were plated on gelatin coated dishes at a density of 45,000 cells/cm^2, and were transfected on the following day with Lipofectamine 3000 according to the manufacturer's instructions for the production of LV-ABR (L3000015, Thermo Fisher Scientific). The LV-ABR plasmid was co-transfected with the third generation packaging vectors pMDLg/pRRE (Addgene 12251), pRSV-Rev (Addgene 12253), and pMd2.G (Addgene 12259) in a 4:2:1:1 ratio. The transfection mix was removed after an overnight incubation, and fresh media was supplied to the cells. The supernatant was collected 48 hours and 72 hours post-transfection and centrifuged at 60,000 x g for 2 hours; the concentrated viral particles were resuspended in Phosphate-Buffered Saline (PBS) buffer overnight.

The virus was subsequently titered in MRC5 human fibroblasts in a serial dilution. Seventy-two hours post-infection cells were collected, the DNA extracted and the number of integrated proviruses/mL was measured by real-time qPCR and compared to a standard curve with primers listed in Suppl. Table 1.

Direct neuronal reprogramming. Low-passage primary human fibroblasts (< P6) from healthy donors (n=3) and ADLD patients [n=3; IT1, IT2 and IT3, (Giorgio *et al.*, 2013)] were plated on Poly-L-Ornitin-Laminin-Fibronectin (Shrigley *et al.*, 2018) coated optical plate (96 well micro-plates, #89626, Ibidi, Martinsried, Germany), at a density of 10,000 cells/cm^2 (Drouin-Ouellet *et al.*, 2017b). The next day (reprogramming day 0, d0), cells were infected with lentiviral particles in the presence of polybrene 4 µg/mL overnight with LV-ABR at a Multiplicity Of Infection (MOI) of

20. On the following day fresh fibroblasts medium substituted the infection medium, and 48 hours later the fibroblasts medium was changed to reprogramming medium from day 2 to 18 (half medium change); from day 18 the medium was switched to maturation medium (Drouin-Ouellet *et al.*, 2017b).

Validation of allele-specific shRNAs in ADLD neurons.

Cells were transduced with lentiviral particles (LV-ASP-T4 shRNA or LV-scramble shRNA) at a MOI of 50 / 80. We tested two different experimental protocols: i) fibroblasts were transduced with LVs at reprogramming day 0 (MOI 50, transduction efficiency of about 75%); ii) fibroblasts were reprogrammed into neurons, and at day 13 of reprogramming (d13) were transduced with lentivirus (MOI 80, transduction efficiency comparable to day 0). At day 20, cells were fixed in PFA 4% for 15 minutes at 4°C for immunocytochemistry. To evaluate the effect of LV-ASP-T4 shRNA, we performed *LMNB1* expression analysis and immunofluorescence evaluations of LMNB1 protein level, nuclear alterations and neurite features (see below).

Validation of allele-specific shRNAs in rat oligodendrocytes cultures overexpressing human LMNB1 coding sequence.

After the shaking procedure, on the first day after plating, part of the cells was transduced with lentiviral particles (LV-ASP-T4 shRNA) at a MOI of 50, that yielded a transduction efficiency of about 60%. The rest of the cells were used as mock controls to define mouse LMNB1 levels. Five days later, transduced cells were transfected with hLMNB1-GFP (allele "T" or "C") construct or a CAGP-AcGFP1 (GFP) empty vector using Lipofectamine 2000 (Thermo Fisher Scientific), following the manufacturer's protocol. Cells were harvested 48 hours post transfection, fixed for 20 minutes in 4% PFA in 0.1 M phosphate buffer (PB) and processed for immunohistochemistry to analyze LMNB1 levels and nuclear alterations.

RNA isolation and quantitative Real Time PCR.

Total RNA was extracted from fibroblasts using the Direct-Zol RNA MiniPrep system (Zymo Research, Irvine, CA) and cDNA was generated using the M-MLV Reverse Transcriptase kit (Invitrogen). The expression levels of *LMNB1*, Ribonucleoprotein, PTB Binding 2 (*RAVER2*), leucine rich repeat containing 15 (*LRRC15*) and the reference gene hydroxymethylbilane synthase (*HMBS*) were measured with predesigned TaqMan assays (Applied Biosystems, *LMNB1*, *RAVER2*, Hs00217122_m1; *LRRC15*, Hs00370056_s1; Hs01059210_m1; *HMBS*, Hs00609297_m1).

Reactions were carried out in triplicate on an ABI 7500 real-time PCR machine using the ABI 2X TaqMan Universal PCR Master Mix II, according to the manufacturer's instructions (Thermo Fisher Scientific).

Allelic discrimination by primer extension assay.

To evaluate the relative amount of the two *LMNB1* alleles after ASP-siRNA treatment, we used an in-house developed primer extension assay based on the SNaPshot System (Thermo Fisher Scientific) (Giorgio et al, 2013). In brief, we extracted total RNA, retrotranscribed cDNA, and amplified a 394 bp region of the *LMNB1* 3'-UTR. After primer extension, reactions were purified using Shrimp Alkaline Phosphatase (SAP, Fermentas), loaded on an ABI-Prism 3730xl DNA analyzer with a GS120-Liz marker, and analyzed using the GeneScan ver 3.7 software (Applied Biosystems, Thermo Fisher Scientific). Using peak height, we calculate the fraction of each allele using the formula Allele "C" = [C/(C+T)]; Allele "T= [T/(C+T)].

Western blot analysis.

Total proteins were extracted from fibroblasts in RIPA buffer. Seven micrograms of protein extracts were run on NuPAGE 4-12% Bis-tris Gel (Invitrogen, Thermo Fisher Scientific), then blotted onto

nitro-cellulose (BIO-RAD, Hercules, CA, USA) in Tris/Glycine buffer with 20% methanol at 4°C for 90 min. Protein transfer efficiency was evaluated using the MemCode Reversible Protein Stain Kit (Pierce Biotechnology Rockford, IL, USA). Lamin B1 and beta-actin were detected using primary anti-lamin B1 (ab16048, Abcam, Cambridge, UK) and anti-b actin (ab8227, Abcam) antibodies and WesternBreeze™ Chemiluminescent Detection Kit (Invitrogen, Thermo Fisher Scientific). Images were captured with a ChemiDoc™ XRS+ System and densitometry analysis was performed with Image Lab™ Software (Bio Rad).

Immunofluorescence.

Fibroblasts. Cells were plated onto coverslips, transfected with siRNAs/LV-shRNAs as previously described, fixed in 4% PFA and immunolabeled as previously described (Giorgio *et al.*, 2015). Samples were immunostained using rabbit polyclonal anti-LMNB1 (ab16048, Abcam) and Alexa Fluor 488 goat anti-rabbit secondary antibody (Thermo Fisher Scientific). The confocal optical sectioning was performed at room temperature (RT) using a Leica TCS SP5 AOBS TANDEM inverted confocal microscope that was equipped with a 40 × HCX PL APO 1.25 oil objective lens. For each experimental point, at least 90 nuclei were analyzed. Three technical replicas were performed. A total of 5,391 nuclei were blindly analyzed.

Reprogrammed neurons and primary OPC cultures. Reprogrammed neurons and primary OPC cultures were processed according to standard immunocytochemical procedures (Boda *et al.*, 2015). Cells were immunostained with polyclonal rabbit anti-LMNB1 (1:2000, as above), mouse monoclonal anti-β-III tubulin (1:800, Promega, Madison USA), or rabbit polyclonal NG2 antiserum (1:400, Millipore). Secondary antibodies were Cy3-(Jackson ImmunoResearch Laboratories, West Grove, PA), Alexa Fluor 488-, and Alexa Fluor 647-conjugated (Molecular Probes Inc, Eugene Oregon). All antibodies were diluted in a PB blocking solution containing 0.3% Triton X-100. To counterstain cell nuclei, we used 4,6-diamidino-2-phenylindole (DAPI, Fluka, Milan, Italy) or TO-

PRO-3 stain (Thermo Fisher Scientific).

In a set-up experiment, we analyzed reprogrammed neurons in one healthy donor and one patient (IT2) to evaluate recombination efficiency (Suppl. Fig.1), and define primary Lamin B1 protein overexpression) and secondary (nuclear alterations) pathological readouts in patients' cells (Suppl. Fig. 1). To this aim, 200-300 cells in two technical replicates were examined for a total of ~600 cells. In the main experiments, we used three healthy donors and three ADLD patients in two biological replicates (see above). About 600 neuronal nuclei for each experimental point were evaluated by densitometric analysis for a total of about 6,700 cells. Two independent experiments with three technical replicates were performed. Images including stacks of the whole cells were acquired with a Leica TCS SP8 confocal microscope and analyzed with NIH ImageJ software to obtain Lamin B1 protein immunofluorescent signal intensity. The nuclear outline was drawn on confocal images based on DAPI or TO-PRO-3 signals, and the integrated density measure of Lamin B1 protein content was obtained. Reprogrammed neurons were distinguished from fibroblasts based on morphological criteria (size and shape of the nucleus, elongated morphology and presence of processes), as validated by anti-β-III tubulin staining (Suppl. Fig. 1). For nuclear alterations, Lamin B1 protein appearance in reprogrammed neurons was classified as follows: homogenous, forming stripes, forming crumples (Suppl. Fig. 1). For evaluation of neurite growth, for each field of view (pictures obtained at 40x magnification) we quantified the number of neurite intersections on a superimposed grid (area of 500 μm^2) and normalized this number by the number of neuronal somata in the corresponding field.

Note that due to the different reporter of shLMNB1 and scramble viral particles, distinct sets of reprogrammed neurons were stained for Lamin B1 protein with different fluorophores (green Alexa Fluo 466, or red Cy3) in order to assess variations in Lamin B1 protein levels. After confirming no significant changes between detected levels of Lamin B1 in ADLD and Ctrl mock conditions with

both the two immunostaining procedures (p= 0.4690), each value for each experimental condition was normalized over the color-matched mock average value. The normalized values were used to compare scramble versus shLMNB1 samples in statistical analyses.

Upon transfection with hLMNB1-GFP, we analyzed OPC cultures as indicated above to define primary (LMNB1 overexpression) and secondary (nuclear alterations) pathological readouts (Suppl. Fig. 2). About 3,300 cells were inspected (two experiments; three technical replicates) and we obtained a transfection efficiency (GFP-positive cells) of about 3%. To examine silencing efficiency, we performed two independent sets of experiments each with three technical replicates analyzing a total of ~2500 cells per round. We performed densitometric analyses of Lamin B1 protein using either anti-Lamin B1 protein immunofluorescent staining or GFP-tag signal.

Statistical Analysis.

Graphics and statistical analysis were performed with Graphpad Prism version 5.00 (Graphpad software, San Diego, CA). Data are presented as mean ± standard error of the mean (SEM). All data were analyzed using two-tailed Mann-Whitney *t-test*. For immunofluorescence experiments, statistical analyses were performed using the mean values for each analyzed field as samples. Values are calculated relative to scramble siRNA/ shRNA using average of at least two independent experiments.

RESULTS

Identification of allele-specific siRNAs.

To exploit the ASP-RNAi strategy, we searched for a frequent SNP within the *LMNB1* transcribed region. We found only four SNPs with a Minor Allele Frequency (MAF) >5% in the dbSNP142 (rs35091677, MAF 0.357 +/- 0.226; rs6875053, 0.068 +/- 0.171; rs1051643, 0.440 +/- 0.162;

rs1051644, 0.495 +/- 0.052). Among these, we chose to target the SNP with the highest MAF, rs1051644, which mapped to the *LMNB1* 3'-UTR. Because the three *LMNB1* alleles in ADLD patients are equally expressed (Giorgio *et al.*, 2013), targeting the non-duplicated allele of the *LMNB1* was expected to reduce expression close to wild-type (see rationale in Fig. 1).

Bioinformatics tools that evaluate siRNA efficiency are poor at predicting allele-specificity (Hohjoh, 2013). Thus, we designed a strategy to screen for siRNAs with the highest capacity for efficient and selective silencing of one allele of the rs1051644 SNP (rationale summarized in Fig. 2A). We used a dual reporter plasmid, containing the *Firefly gene* fused to part of the *LMNB1-3'-UTR* and the *Renilla* luciferase gene. To test all the 19 possible siRNAs (19 + 2 bp geometry) that targeted the "C" or the "T" allele of rs1051644 (Suppl. table 2).

The results are summarized in Fig. 2B and 2C. We identified three non-efficient siRNAs (<70% reduction of the target allele at 30 nM; SNP positions 2, 8 and 13) and 16 efficient siRNAs (SNP positions 1, 3-7, 9-12, 14-19). Only five of these showed statistically different allele specificity, at both concentrations tested (Fig. 2B and 2C; SNP positions 3-6, 9). Based on ASP-siRNA definition (Allen *et al.*, 2013), we further selected siRNAs 3-5, and 9, which strongly knocked down the target allele at the lower concentration tested while minimally affecting the non-target allele at the highest concentration tested (Suppl. table 3).

ASP-siRNAs restored physiological LMNB1 levels, and ameliorated ADLD cellular phenotypes in patients' fibroblasts.

Human ADLD fibroblasts represent a genetically accurate model to assess siRNA allele specificity (Scholefield *et al.*, 2014). These fibroblasts have the genomic context with *LMNB1* duplication, are easy to manipulate, and allow the readout for ADLD-associated phenotypes, such as nuclear blebs and altered gene expression (Ferrera *et al.*, 2014; Bartoletti-Stella *et al.*, 2015; Giorgio *et al.*, 2015).

We evaluated the efficiency of selected siRNAs by measuring *LMNB1 vs. HMBS* (reference gene)

by RT-qPCR in ADLD fibroblasts (Fig. 3A). We observed that ASP-siRNAs 3-5 and 9 significantly reduced *LMNB1* mRNA levels both at 40 nM (Suppl. table 4) and 100 nM (Fig. 3A and Suppl. table 4). Interestingly, three ASP-siRNAs (3, 4 and 9 at 100 nM) restored *LMNB1* expression to physiological levels. At the same concentrations (30 nM and 100 nM), the non-allele specific siRNA (*LMNB1* CTRL+) reduced *LMNB1* expression close to zero (Suppl. table 4).

We accurately evaluated allele-specificity of these four selected siRNAs exploiting a primer extension assay previously developed by our group (Giorgio *et al.*, 2013) (Fig. 3B). ASP-siRNAs T3, T4 and T9 preferentially silenced the matched "T" allele, at both tested concentrations. On the other hand, only C3 and C4 siRNAs showed significant allele specificity for the matched *LMNB1* allele (Fig. 3B, Suppl. table 5). Both siRNAs with the SNP at position 5 did not show statistically significant allele-specificity (T5 and C5 in Fig. 3B, Suppl. table 5). Overall, these results demonstrated the efficiency and allele specificity of T3, T4, T9, C3 and C4 siRNAs.

Next, we verified if the reduction in *LMNB1* mRNA correlated with decreased protein. All ASP-siRNAs (SNP positions 3-5 and 9) significantly reduced LMNB1 protein compared to scramble siRNA ($p < 0.0001$; Suppl. table 6). Most interestingly, the reduction mediated by ASP-siRNAs at positions 3-5 restored LMNB1 protein to physiological values (Fig. 3C and 3D; Suppl. table 6).

Furthermore, to evaluate the therapeutic potential in ADLD of the selected ASP-siRNAs, they were evaluated for their ability to abrogate *LMNB1*-overexpression dependent cellular phenotypes, such as nuclear blebs (Ferrera *et al.*, 2014; Giorgio *et al.*, 2015) and transcriptome alterations (Bartoletti-Stella *et al.*, 2015) in patients' fibroblasts. These experiments were performed after incubation for 120 hours, confirming the ability of ASP-siRNA to restore physiological LMNB1 expression level at this time point (Suppl. table 4).

By fluorescent microscopy, we blindly evaluated 5,391 nuclei and scored them as regular (oval/spherical) or misshaped (irregular profile, blebs and invaginations). We detected ~10% of nuclear abnormalities in healthy controls and ~40% in patients ($p < 0.0001$; Fig. 4A scramble;

Suppl. table 7). ASP silencing reduced the percentage of misshaped nuclei in ADLD fibroblasts to close to that of wild-type (Fig. 4A-D; Suppl. table 7).

To evaluate transcriptome alterations, we assessed the ability of the ASP-siRNAs to modulate *RAVER2* and *LRRC15* mRNAs, which are overexpressed in ADLD patients (Bartoletti-Stella *et al.*, 2015). Cells treated with ASP-siRNAs showed a statistically significant reduction of *RAVER2* (Fig. 4E; Suppl. table 7; $p < 0.005$) and *LRRC15* expression (Fig. 4F; Suppl. table 7; $p < 0.005$).

ASP-siRNA treatment ameliorated ADLD-specific cellular phenotypes in disease-relevant cellular models.

Disease-relevant cellular and animal models are essential to study disease progression and to screen potential therapies. To this aim, we have further validated ASP-RNAi strategy as ADLD therapy into directly-reprogrammed ADLD neurons and rat oligodendrocyte cultures overexpressing hLMNB1.

Validation of the therapeutic potential of ASP-siRNA in reprogrammed ADLD neurons.

Fibroblasts from three ADLD patients and three healthy subjects were directly-reprogrammed into neurons. About 60% of cells (58% in controls and 64% in patients-derived cells) were effectively reprogrammed as shown by β-III tubulin positive staining (Suppl. Fig. 1A). As expected, ADLD neurons showed increased LaminB1 protein level compared to control neurons ($p< 0.0001$), an increased number of nuclear abnormalities ($p= 0.0034$) and neurite outgrowth ($p< 0.0001$) (Suppl. Fig. 1E).

To validate our ASP-RNAi strategy, neurons were transduced at two different time points (reprogramming day 0, and day 13) with lentiviral particles (LV-shLMNB1 or LV-scramble shRNA) at a MOI of 50 or 80. Untreated (mock) or treated with LV-scramble shRNA (scramble) ADLD neurons showed an increased Lamin B1 protein level compared to controls (mock p=

0.0003; scramble p> 0.0001. Fig. 5A-B; Suppl. table 8). Notably, neuron transduction with scramble particles does not influence Lamin B1 protein level compared to non-infected cells (p=0.8696; Fig. 5A-B; Suppl. table 8). The treatment at day 0 with the allele-specific shRNA-T4 (shLMNB1 d0) reduces Lamin B1 protein of about 30% in ADLD neurons compared to scramble shRNA (p< 0.0001), ameliorates ADLD-specific neuronal phenotypes such as nuclear anomalies (p< 0.0001) and neurite growth (p< 0.0001)(Fig. 5C-D; Suppl. table 8). On the other hand, the treatment at d13 (shLMNB1 d13) induces a minor but significant reduction of Lamin B1 levels (p= 0.0316) and partly improves the cellular phenotypes (crumpled nuclei; p= 0.0100)(Fig. 5A-D and Suppl. table 8).

Validation of the therapeutic potential of ASP-siRNA in rat oligodendrocyte cultures overexpressing hLMNB1.

Primary Oligodendrocyte Precursors Cells (OPCs) were transduced with lentiviral particles (shLMNB1) at a MOI of 50. Five days later, OPCs were transfected with GFP-tagged human Lamin B1 expression plasmids containing the "T" allele (matched allele) or the "C" allele (non-matched allele) of the target SNP (h*LMNB1*-T and h*LMNB1*-C, respectively). When transfected with the GFP-tagged human Lamin B1, OPCs (GFP positive, GFP+) consistently showed increased LaminB1 protein level, as detected with immunostaining, compared to non-transfected cells (GFP negative, GFP-, mock) (p= 0.0177; Suppl. Fig. 2B-C), and presented nuclear abnormalities (Suppl. Fig. 2D I-IV). Namely, nuclei of GFP+ OPCs showed a unique striped or shrinked pattern suggestive of ongoing nuclear fragmentation (Suppl. Fig. 2D III,IV). This feature occurred with a frequency of about 5% in OPCs overexpressing human Lamin B1 while it was virtually absent in GFP- cells (Suppl. Fig. 2D I,II). These data corroborated our oligodendrocyte culture as an appropriate ADLD-relevant cellular model.

OPCs overexpressing the hLMNB1-T allele and treated with the allele-specific shRNA-T4

(shLMNB1; matched siRNA) showed a strong reduction of Lamin B1 protein level ($p < 0.0001$. Fig. 6; Suppl. table 9). Interestingly, OPCs overexpressing the hLMNB1-C allele (non-matched allele) and treated with the LV-shASP-T4 did not show any difference compared to scramble ($p = 0.1960$. Fig. 6; Suppl. table 9), substantiating the allele-specificity of our therapeutic molecule. Finally, ADLD-specific nuclear anomalies (reported in Suppl. Fig.2) appear to be reduced to about one third when the "T" allele was silenced while they were essentially maintained in cells overexpressing the "C" allele. We obtained comparable results evaluating Lamin B1 levels by both immunostaining and fluorescence of the GFP reporter encoded by the transfected plasmid (Fig. 6; Suppl. table 9).

DISCUSSION

Autosomal Dominant adult-onset demyelinating LeukoDystrophy (ADLD) is a fatal neurological disorder for which no treatment is available. Because the age of onset is usually beyond 35 years of age, this disease represents an ideal candidate for a treatment that could be administered in the pre-symptomatic phase. The brain and spinal cord MRI findings can precede clinical manifestations by years, thus monitoring patients may allow starting the treatment when the first MRI signs occur (Nahhas, 2016).

As ADLD is caused primarily by *LMNB1* gene duplication-mediated overexpression, the treatment of choice would be a drug capable of reducing its expression. On the other hand, excessive gene knockdown may have deleterious effects, as shown in cellular and mouse models (Liu *et al.*, 2000; Harborth *et al.*, 2001; Vergnes *et al.*, 2004; Ji *et al.*, 2007; Coffinier *et al.*, 2010; Bartoletti-Stella *et al.*, 2015; Giacomini *et al.*, 2016). Given this context, a fine modulation of Lamin B1 expression is required for an effective ADLD therapeutic option.

We reasoned that Allele-SPecific silencing by interfering RNA (ASP-RNAi) was the best choice, given that it can specifically inhibit the expression of one of the three *LMNB1* alleles in a *LMNB1*-duplicated patient, avoiding a potentially excessive and harmful *LMNB1* knockdown.

ADLD patients have three, equally expressed, *LMNB1* alleles that we discriminated exploiting the rs1051644 SNP. Thus, to restore physiological *LMNB1* levels, we choose to target the non-duplicated allele, maintaining transcriptionally active only two copies of the gene, as in normal subjects.

Identification of efficient and specific ASP-siRNAs required an *in vitro* screening using a dual-reporter vector challenged with a library of all possible 19 siRNAs targeting rs1051644. We found three ASP-siRNAs able to silence the target allele with minimal suppression of the non-target one (positions 3, 4 and 9). In treated ADLD-derived fibroblasts, we proved *LMNB1* expression and protein levels were restored to normal levels.

Thus, we planned testing the effects of ASP-siRNAs on LMNB1-connected biological changes. Lamins are essential building blocks of the nuclear lamina and mechanically enforce the nuclear morphology (de Leeuw *et al.*, 2017). Generally, disease-causing mutant lamins lead to abnormal nuclear morphology that is visible on the cellular level. In lamin knockout experiments, cells appear to have small fragile nuclei, decreased nuclear stiffness and nuclear shape can be affected (Vergnes *et al.*, 2004; Lammerding *et al.*, 2006; Coffinier *et al.*, 2011; Shimi *et al.*, 2011). Lamin overexpression causes blebs and invaginations of the nuclear envelope (Prufert *et al.*, 2004; Friedl *et al.*, 2011) and increases nuclear stiffness (Ferrera *et al.*, 2014). Following our treatment with ASP-siRNAs, we showed that ADLD fibroblasts quickly reverted the nuclear shape to regular nuclei.

Beyond their structural role, a fraction of lamins also reside throughout the nuclear interior where they have important roles in essential cellular processes such as transcription, DNA replication, cell cycle progression, and chromatin organization (Dechat *et al.*, 2010; Buchwalter *et al.*, 2019). We could demonstrate that the expression of two known genes affected by LMNB1 levels, *RAVER2* and *LRRC15,* significantly decreased after treatment. Corroborating the clinical relevance of ASP-siRNAs, we previously reported that *RAVER2* is directly involved in ADLD pathogenesis: its

overexpression results in abnormal splicing patterns of several phosphotyrosine binding domain (PTB)-target genes and of Proteolipid Protein 1 (PLP1), the predominant protein component of myelin (Bartoletti-Stella *et al.*, 2015), previously demonstrated to be implicated in ADLD (Heng *et al.*, 2013).

Overall, our results pinpoint two ASP-siRNAs (positions 3 and 4) able to silence specifically one of the three *LMNB1* alleles in ADLD-cells, restoring physiological levels of mRNA and protein and ameliorating disease-relevant cellular phenotypes in patients' fibroblasts.

To demonstrate ASP-silencing efficacy in cell types more relevant to ADLD, we generated two cellular models: 1) neurons directly reprogrammed from human fibroblasts; 2) rat oligodendrocyte precursor cells (OPCs) overexpressing the human *LMNB1*. We proved that both cellular models presented increased Lamin B1 levels compared to control cells and showed ADLD-specific cellular phenotypes, supporting their relevance as *in vitro* preclinical tools.

Both cellular models were treated with the most efficient ASP-molecule (LV-ASP-T4 shRNA).

The treatment reduced Lamin B1 protein level in both models and ameliorated ADLD-specific cellular abnormalities, validating the therapeutic potential of our RNA molecule. Furthermore, rat OPCs overexpressing human Lamin B1 allowed us to further assess the allele-specificity of our strategy. Indeed, the LV-ASP-T4 shRNA effectively silenced only cells overexpressing the human LMNB1 allele carrying the "T" allele of the targeted rs1051644 SNP (matched allele).

ADLD is a late-onset disease with a thirty year-long preclinical phase. We think it would be more effective to treat patients in this pre-symptomatic window, in order to prevent the Lamin B1-overexpression dependent cellular degeneration in brain. To prove our hypothesis, neurons were treated at two different time points. As expected, treating cells at the start of the reprogramming process (day 0) showed a significant improvement of ADLD-specific neuronal phenotypes, compared to the treatment performed at reprogramming day 13 (d13), which only partially ameliorates cellular phenotypes.

Following these results, at least one RNA molecule (ASP-T4) is approved for a further step of validation, namely *in vivo* treatment of animal models. Our ASP-silencing strategy requires a fully humanized mouse carrying three human *LMNB1* alleles, recapitulating ADLD phenotypes and heterozygous for the SNP targeted by ASP-siRNAs (rs1051644). This mouse model would mimic the precise genomic context of *LMNB1* duplication found in patients and would allow the *in vivo* evaluation of efficacy and selectivity (allele specificity) of the identified siRNAs. Unfortunately, both the two mouse models currently available (*Lmnb1*^{BAC} and *PLP*-LMNB1^{Tg})(Heng *et al.*, 2013; Rolyan *et al.*, 2015) are not suitable for this experiment. The *Lmnb1*^{BAC} mice overexpress a murine multiple lamin B1 transgene, not targetable by our ASP-siRNA strategy. In the *PLP-LMNB1*^{Tg} mouse, the human overexpressed *LMNB1* gene does not contain the 3'-UTR, where the rs1051644 maps.

To overcome this obstacle, we are working to generate a chimeric mouse model in which oligodendroglial cells and myelin will be patient-derived, by performing multifocal neonatal engraftment in immunocompromised dysmyelinated mice (*shiverer mice*) with OPCs derived from patients' hiPSCs, as described by (Wang *et al.*, 2013; Osipovitch *et al.*, 2019). This mouse model would represent a unique system to evaluate the *in vivo* preclinical efficacy of ASP-siRNAs in ADLD.

Delivery of ASP-siRNA to their target tissue and cellular internalization are still major challenges that limit their full use in therapy. Recently, clinically relevant delivery of siRNAs has been achieved exploiting two main classes of vehicles: non-viral (e.g., liposomes, exosomes, polymeric nanoparticles) or viral vectors (herpes simplex virus type 1, adenovirus, adeno-associated virus and lentivirus) (van den Boorn *et al.*, 2011; Choudhury *et al.*, 2016; Mishra *et al.*, 2017). Among the latter, adeno-associated type 9 (AAV-9) viruses show an efficient tropism for brain cells both *in vitro* and *in vivo*, including neurons, oligodendrocytes and glial cells (Foust *et al.*, 2009; Aschauer *et al.*, 2013; Bucher *et al.*, 2014; Dufour *et al.*, 2014). Moreover, AAV-9 viruses pass the blood-

brain barrier, present a low risk of insertional mutagenesis and trigger diminished immune responses (Foust *et al.*, 2009; Aschauer *et al.*, 2013; Dufour *et al.*, 2014; Gong *et al.*, 2015; Saraiva *et al.*, 2016). AAV-9 viruses have been employed in different clinical trials, and are thus an interesting delivery system for ASP-siRNA in ADLD (Foust *et al.*, 2009; Aschauer *et al.*, 2013; Dufour *et al.*, 2014; Gong *et al.*, 2015; Saraiva *et al.*, 2016). Of note, several reports showed that nanoparticle-linked siRNA can be delivered *in vivo* into the brain by intranasal administration to knock down target proteins into neurons, microglia and astrocytes, opening new routes of administration distinct from the more invasive intrathecal injection-mediated delivery strategy (Mistry *et al.*, 2009; Biddlestone-Thorpe *et al.*, 2012; Rodriguez *et al.*, 2017).

Our work represents a proof-of-concept for the use of ASP-siRNA in genetic disorders associated with gene(s) duplication, and could be applied to rare conditions such as Pelizaeus-Merzbacher disease, Charcot-Marie-Tooth type 1A and Rett syndrome (Table 1). Aside from single-gene diseases, disorders associated with large genomic copy number gains might be potentially treated by ASP-siRNA whenever the pathological phenotype is associated to the overexpression of different dosage-sensitive genes, requiring a multiple-target ASP-siRNA strategy.

Overall, our work demonstrated that ASP-silencing is a suitable and promising therapeutic option for ADLD, prompting further *in vivo* studies to validate our results before clinical trials. Moreover, our results have a broad translational value extending to several pathological conditions linked to gene copy number variations.

ACKNOWLEDGEMENTS

We thank Dr. Malin Parmar at the University of Lund (Sweden) for providing plasmid vectors used in fibroblasts-to-neuron reprogramming. We are also indebted to the ADLD family members who participated in this study. Patent approved for the ASP-siRNA sequences n. 102017000121288

entitled “RNA interference mediated therapy for neurodegenerative diseases”.

FUNDING

The work was supported by the Fondazione Umberto Veronesi (post-doctoral fellowship 2017 to EG), Ricerca locale MURST ex 60% and the “Associazione E. E. Rulfo per la ricerca biomedica” to ABrusco. Ricerca locale MURST ex 60% to ABuffo; Marie Curie Individual Fellowship to PRdVC (DISMOD-HD); Ministero dell’Istruzione, dell’Università e della Ricerca – MIUR “Dipartimenti di Eccellenza 2018–2022” to Department of Medical Sciences (Project D15D18000410001) and Department of Neuroscience Rita Levi Montalcini.

LEGENDS TO FIGURES

Fig. 1. Overview for the Allele Specific siRNA (ASP-siRNA) strategy.

In Autosomal Dominant LeukoDystrophy (ADLD) patients, three copies of the lamin B1 (*LMNB1*) gene (rounded rectangles) are present due to a genomic duplication. We show some of the possible genomic conformations for the rs1051644 alleles that can have a "C" (light blue) or a "T" (green) polymorphic base. Below, analysis of the *LMNB1* mRNA (curved line) from previous studies show an equal expression of the three alleles (Giorgio *et al.*, 2013).

Silencing of the non-duplicated allele by ASP-siRNA is the best strategy to reduce the amount of *LMNB1* without excessively downregulating the gene. The histograms show that in an optimal situation, following ASP-siRNA treatment, the amount of *LMNB1* is reduced to the level of wild-type due to the specific knockdown of one allele.

Fig. 2. Allele Specific siRNA screening.

In panel A, the rationale used to identify efficient and allele-specific siRNA. Using a psiCHECK dual luciferase vector, we cloned part of the 3'-UTR of *LMNB1* downstream to the *hRluc* gene (green rectangle) used as reference. The hluc gene (*Renilla*, yellow rectangle) in the plasmid is used to normalize the transfection efficiency (T7 and HVV-TK indicate promoter types). Two vectors were generated, one with the "T" and one with the "C" allele at rs1051644.

The reporter vector was challenged with each of 19 siRNA containing the rs1051644 "C" or "T" allele in one of the 19 possible positions (see Suppl. table 2 for details) at two different concentrations (12.5 nM, panel B; 30 nM, panel C). A scramble siRNA and a siRNA against *hRluc* were used as negative and positive controls, respectively. Ideally, the best siRNA should completely abrogate the matched allele, leaving the unmatched allele unchanged (panel A, histograms).

Results of this screening are reported in panels B and C. Numbers on the X-axis indicate the position of the mismatch on the siRNA. CTRL+ indicate a non-allele specific *LMNB1* siRNA.

Statistical significant differences (asterisks) between matched (blue) and unmatched (orange) siRNAs are reported ($p<0.05$: *; $p<0.01$: **; $p<0.001$: ***; two-tailed, Mann-Whitney). The most efficient and allele-specific siRNAs are circled.

Fig. 3. Primary readouts of ASP-siRNA efficacy.

ADLD fibroblasts with the "C" allele on the duplicated *LMNB1* copy were treated with 100 nM ASP-siRNAs against the "T" allele of rs1051644 and *vice versa* for 48 hours; mock = untreated cells. Four different ADLD cell lines and three age-matched controls were tested. At least three independent technical replicas were performed. In panel A, evaluation of total *LMNB1* mRNA levels by quantitive RT-PCR (*LMNB1* vs *HMBS*). Fold change and SEM (bars) are reported. Statistical significance is given comparing ADLD vs scramble ($p<0.05$: *; $p<0.01$: **; $p<0.001$: ***; two-tailed, Mann-Whitney). In panel B, evaluation of allele-specific expression using primer extension assay (allele C versus allele T, percentage). Mean ± SEM (bars) are reported. Statistical significant values were evaluated comparing ADLD vs scramble ($p<0.01$: **; $p<0.001$: ***; two-tailed, Mann-Whitney).

In panels C and D, evaluation of total LMNB1 protein by western blot (LMNB1 vs β-actin). Immunostaining with anti-LMNB1 and anti-β-actin antibodies are shown as exemplification of the analysis in panel C. Fold-change densitometric data and SEM (bars) are shown in panel D. Statistical significant differences (asterisks) is reported for ADLDs vs. scramble ($p<0.05$: *; $p<0.01$: **; $p<0.001$: ***; two-tailed, Mann-Whitney). D- Schematic drawing showing the genomic structure of ADLD patients used in the experiments in reference to rs1051644.

Fig. 4. Secondary readouts of ASP-siRNA efficacy.

ADLD fibroblasts with the "C" allele on the duplicated *LMNB1* copy were treated with 100 mM ASP-siRNAs against the "T" allele of the SNP and *vice versa* for 120 hours. Four different ADLD

cell lines and three age-matched controls were tested. At least three independent experiments were performed.

Nuclear shape anomalies were evaluated by fluorescent microscopy after LMNB1 staining. A total of 5,391 nuclei were evaluated in blind. Fold-change and SEM (bars) are shown in panel A. Statistical significant values show differences between ADLD and scramble ($p<0.001$: ***; $p<0.0001$: ****; two-tailed, Mann-Whitney). Nuclei from a control line treated with scramble siRNA (CTRL scramble, panel B) and an ADLD line treated with scramble siRNA (ADLD scramble, panel C) or with ASP-siRNAs (ADLD ASP-siRNA, panel D) are shown as exemplification of the analysis. Blebs (asterisk) and invaginations (arrow heads) are highlighted.

E-F. Histograms show quantitative real-time PCR results for *RAVER2* mRNA levels (panel E; *RAVER2* vs *HMBS*) and *LRRC15* (panel F; *LRRC15* vs *HMBS*). Fold change and SEM (bars) are reported. Statistical significant differences (asterisks) is given for ADLDs vs. scramble ($p<0.02$: **; $p<0.001$: ***; $p<0.0001$: ****; two-tailed, Mann-Whitney).

Fig. 5. Validation of ASP-RNAi in reprogrammed neurons.

Panel A shows neurons directly reprogrammed from fibroblasts of ADLD patients (ADLDs) or healthy subjects (CTRLs), stained for β-III tubulin. Neurons were cultured with no treatments (mock), or transduced with either scramble lentiviral particles (scramble) or with shLMNB1 viruses at two different time points, reprogramming day 0 or day 13 (shLMNB1 d0; shLMNB1 d13). For each panel a 2 fold magnified inset is shown. Note that labelling for Lamin B1 protein is presented in green or red, in accordance with the corresponding fluorescent reporter encoded by the infecting viral particles. Panels B, C and D show, respectively, quantifications of Lamin B1 protein levels, neurite growth and nuclear anomalies in cells untreated (mock), infected with LV-scramble shRNA (scramble) or with the ASP-vector at d0 (shLMNB1 d0) or d13 (shLMNB1 d13). Examples of nuclei corresponding to the categories represented in Panel D are shown in Suppl. Fig. 1 (Panel E).

Statistically significant differences (asterisks) are shown for comparisons between ADLDs shLMNB1 vs. ADLD scramble (panel B: Mann-Whitney t-test ;****, p< 0.0001; *, p= 0.0316; panel C: Mann-Whitney t-test; ****, p< 0.0001; **, p= 0.0030; panel D: Mann-Whitney t-test; d0, crumpled nuclei, ****, p< 0.0001; d0 striped nuclei, **, p= 0.0046; d13 crumpled nuclei, *, p= 0.0100; ns, p> 0.05). Details of statistical analysis for all comparisons are reported in Suppl. Table 8. Error bars: SEM. Staining: Lamin B1 (green or red), β-III tubulin (green or red), LV-scramble (green), ASP-vector (red), cell nuclei/TO-PRO-3 (blue). Scale bars are shown.

Fig. 6. Validation of ASP-RNAi in OPCs overexpressing hLMNB1.

Panel A shows OPCs transfected to overexpress the 'T' (h*LMNB1*-T; up) or the "C" (h*LMNB1*-C; down) allele of the GFP-tagged human LMNB1 (yellow arrows). The human GFP-tagged Lamin B1 protein (green) localizes to the cell nuclei (DAPI staining, blue), as expected. Cells were cultured with no treatments (mock; untreated: left) or transduced with the ASP-vector (shLMNB1; treated: right). White arrows indicate effectively transfected (GFP+, green) and transduced (red) cells. For each panel a 2× magnified inset displaying GFP-tagged Lamin B1 is shown. OPCs, oligodendrocyte progenitor cells. Staining: hLamin B1-GFP protein (green), cells transduced with LV-shLMNB1 (shLMNB1, red), nuclei, DAPI (blue). Scale bars are shown. Panel B shows quantifications of total Lamin B1 protein levels obtained by analyses of human and mouse Lamin B1 immunostaining in cells untreated (GFP-; mock), transfected with the GFP-tagged human Lamin B1 "T" allele (GFP+ hLMNB1-T) or the GFP-tagged human Lamin B1 "C" allele (GFP+ hLMNB1-C), or transfected and treated with the LV-shLMNB1 (shLMNB1). Panel C shows quantifications of human Lamin B1 protein levels based on tagged GFP fluorescence in cells transfected with the GFP-tagged human Lamin B1 "T" allele (GFP+ hLMNB1-T) or the GFP-tagged human Lamin B1 "C" allele (GFP+ hLMNB1-C) or transfected (GFP+) and infected with

the LV-shLMNB1 (shLMNB1). Statistically significant differences are shown for GFP+ shLMNB1 vs. GFP+ or GFP- cells (Mann-Whitney t-test ;****, $p < 0.0001$; ns, $p > 0.05$).

REFERENCES

Allen EH, Atkinson SD, Liao H, Moore JE, Leslie Pedrioli DM, Smith FJ, *et al.* Allele-specific siRNA silencing for the common keratin 12 founder mutation in Meesmann epithelial corneal dystrophy. Investigative ophthalmology & visual science 2013; 54(1): 494-502.

Alves S, Nascimento-Ferreira I, Auregan G, Hassig R, Dufour N, Brouillet E, *et al.* Allele-specific RNA silencing of mutant ataxin-3 mediates neuroprotection in a rat model of Machado-Joseph disease. PLoS One 2008; 3(10): e3341.

Antonarakis SE. Down syndrome and the complexity of genome dosage imbalance. Nat Rev Genet 2017; 18(3): 147-63.

Aschauer DF, Kreuz S, Rumpel S. Analysis of transduction efficiency, tropism and axonal transport of AAV serotypes 1, 2, 5, 6, 8 and 9 in the mouse brain. PLoS One 2013; 8(9): e76310.

Bartoletti-Stella A, Gasparini L, Giacomini C, Corrado P, Terlizzi R, Giorgio E, *et al.* Messenger RNA processing is altered in autosomal dominant leukodystrophy. Hum Mol Genet 2015; 24(10): 2746-56.

Biddlestone-Thorpe L, Marchi N, Guo K, Ghosh C, Janigro D, Valerie K, *et al.* Nanomaterial-mediated CNS delivery of diagnostic and therapeutic agents. Advanced drug delivery reviews 2012; 64(7): 605-13.

Boda E, Di Maria S, Rosa P, Taylor V, Abbracchio MP, Buffo A. Early phenotypic asymmetry of sister oligodendrocyte progenitor cells after mitosis and its modulation by aging and extrinsic factors. Glia 2015; 63(2): 271-86.

Bucher T, Dubreil L, Colle MA, Maquigneau M, Deniaud J, Ledevin M, *et al.* Intracisternal delivery of AAV9 results in oligodendrocyte and motor neuron transduction in the whole central nervous system of cats. Gene Ther 2014; 21(5): 522-8.

Buchwalter A, Kaneshiro JM, Hetzer MW. Coaching from the sidelines: the nuclear periphery in genome regulation. Nat Rev Genet 2019; 20(1): 39-50.

Bumcrot D, Manoharan M, Koteliansky V, Sah DW. RNAi therapeutics: a potential new class of pharmaceutical drugs. Nature chemical biology 2006; 2(12): 711-9.

Camps J, Wangsa D, Falke M, Brown M, Case CM, Erdos MR, *et al.* Loss of lamin B1 results in prolongation of S phase and decondensation of chromosome territories. FASEB J 2014; 28(8): 3423-34.

Choudhury SR, Fitzpatrick Z, Harris AF, Maitland SA, Ferreira JS, Zhang Y, *et al.* In Vivo Selection Yields AAV-B1 Capsid for Central Nervous System and Muscle Gene Therapy. Mol Ther 2016; 24(7): 1247-57.

Coelho T, Adams D, Silva A, Lozeron P, Hawkins PN, Mant T, *et al.* Safety and efficacy of RNAi therapy for transthyretin amyloidosis. N Engl J Med 2013; 369(9): 819-29.

Coffeen CM, McKenna CE, Koeppen AH, Plaster NM, Maragakis N, Mihalopoulos J, *et al.* Genetic localization of an autosomal dominant leukodystrophy mimicking chronic progressive multiple sclerosis to chromosome 5q31. Hum Mol Genet 2000; 9(5): 787-93.

Coffinier C, Chang SY, Nobumori C, Tu Y, Farber EA, Toth JI, *et al.* Abnormal development of the cerebral cortex and cerebellum in the setting of lamin B2 deficiency. Proc Natl Acad Sci U S A 2010; 107(11): 5076-81.

Coffinier C, Jung HJ, Nobumori C, Chang S, Tu Y, Barnes RH, 2nd, *et al.* Deficiencies in lamin B1 and lamin B2 cause neurodevelopmental defects and distinct nuclear shape abnormalities in neurons. Mol Biol Cell 2011; 22(23): 4683-93.

Davis ME, Zuckerman JE, Choi CH, Seligson D, Tolcher A, Alabi CA, *et al.* Evidence of RNAi in humans from systemically administered siRNA via targeted nanoparticles. Nature 2010; 464(7291): 1067-70.

de Fougerolles A, Vornlocher HP, Maraganore J, Lieberman J. Interfering with disease: a progress report on siRNA-based therapeutics. Nature reviews Drug discovery 2007; 6(6): 443-53.

de Leeuw R, Gruenbaum Y, Medalia O. Nuclear Lamins: Thin Filaments with Major Functions. Trends Cell Biol 2017.

Dechat T, Gesson K, Foisner R. Lamina-independent lamins in the nuclear interior serve important functions. Cold Spring Harb Symp Quant Biol 2010; 75: 533-43.

Deshpande A, Weiss LA. Recurrent reciprocal copy number variants: Roles and rules in neurodevelopmental disorders. Dev Neurobiol 2018; 78(5): 519-30.

DeVincenzo J, Lambkin-Williams R, Wilkinson T, Cehelsky J, Nochur S, Walsh E, *et al.* A randomized, double-blind, placebo-controlled study of an RNAi-based therapy directed against respiratory syncytial virus. Proc Natl Acad Sci U S A 2010; 107(19): 8800-5.

Drouin-Ouellet J, Lau S, Brattas PL, Rylander Ottosson D, Pircs K, Grassi DA, *et al.* REST suppression mediates neural conversion of adult human fibroblasts via microRNA-dependent and -independent pathways. EMBO Mol Med 2017a; 9(8): 1117-31.

Drouin-Ouellet J, Pircs K, Barker RA, Jakobsson J, Parmar M. Direct Neuronal Reprogramming for Disease Modeling Studies Using Patient-Derived Neurons: What Have We Learned? Frontiers in neuroscience 2017b; 11: 530.

Dufour BD, Smith CA, Clark RL, Walker TR, McBride JL. Intrajugular vein delivery of AAV9-RNAi prevents neuropathological changes and weight loss in Huntington's disease mice. Mol Ther 2014; 22(4): 797-810.

Dykxhoorn DM, Lieberman J. Knocking down disease with siRNAs. Cell 2006; 126(2): 231-5.

Eldridge R, Anayiotos CP, Schlesinger S, Cowen D, Bever C, Patronas N, *et al.* Hereditary adult-onset leukodystrophy simulating chronic progressive multiple sclerosis. N Engl J Med 1984; 311(15): 948-53.

Ferrera D, Canale C, Marotta R, Mazzaro N, Gritti M, Mazzanti M, *et al.* Lamin B1 overexpression increases nuclear rigidity in autosomal dominant leukodystrophy fibroblasts. FASEB J 2014; 28(9): 3906-18.

Foust KD, Nurre E, Montgomery CL, Hernandez A, Chan CM, Kaspar BK. Intravascular AAV9 preferentially targets neonatal neurons and adult astrocytes. Nat Biotechnol 2009; 27(1): 59-65.

Friedl P, Wolf K, Lammerding J. Nuclear mechanics during cell migration. Current opinion in cell biology 2011; 23(1): 55-64.

Giacomini C, Mahajani S, Ruffilli R, Marotta R, Gasparini L. Lamin B1 protein is required for dendrite development in primary mouse cortical neurons. Mol Biol Cell 2016; 27(1): 35-47.

Giorgio E, Robyr D, Spielmann M, Ferrero E, Di Gregorio E, Imperiale D*, et al.* A large genomic deletion leads to enhancer adoption by the lamin B1 gene: a second path to autosomal dominant adult-onset demyelinating leukodystrophy (ADLD). Hum Mol Genet 2015; 24(11): 3143-54.

Giorgio E, Rolyan H, Kropp L, Chakka AB, Yatsenko S, Gregorio ED*, et al.* Analysis of LMNB1 Duplications in Autosomal Dominant Leukodystrophy Provides Insights into Duplication Mechanisms and Allele-Specific Expression. Hum Mutat 2013; 34(8): 1160-71.

Gong Y, Mu D, Prabhakar S, Moser A, Musolino P, Ren J*, et al.* Adenoassociated virus serotype 9-mediated gene therapy for x-linked adrenoleukodystrophy. Mol Ther 2015; 23(5): 824-34.

Guelen L, Pagie L, Brasset E, Meuleman W, Faza MB, Talhout W*, et al.* Domain organization of human chromosomes revealed by mapping of nuclear lamina interactions. Nature 2008; 453(7197): 948-51.

Harborth J, Elbashir SM, Bechert K, Tuschl T, Weber K. Identification of essential genes in cultured mammalian cells using small interfering RNAs. J Cell Sci 2001; 114(Pt 24): 4557-65.

Haussecker D. The business of RNAi therapeutics. Hum Gene Ther 2008; 19(5): 451-62.

Heng MY, Lin ST, Verret L, Huang Y, Kamiya S, Padiath QS*, et al.* Lamin B1 mediates cell-autonomous neuropathology in a leukodystrophy mouse model. J Clin Invest 2013; 123(6): 2719-29.

Hohjoh H. Disease-causing allele-specific silencing by RNA interference. Pharmaceuticals 2013; 6(4): 522-35.

Jacquemont S, Reymond A, Zufferey F, Harewood L, Walters RG, Kutalik Z*, et al.* Mirror extreme BMI phenotypes associated with gene dosage at the chromosome 16p11.2 locus. Nature 2011; 478(7367): 97-102.

Ji JY, Lee RT, Vergnes L, Fong LG, Stewart CL, Reue K*, et al.* Cell nuclei spin in the absence of lamin b1. J Biol Chem 2007; 282(27): 20015-26.

Jiang YQ, Wang XL, Cao XH, Ye ZY, Li L, Cai WQ. Increased heat shock transcription factor 1 in the cerebellum reverses the deficiency of Purkinje cells in Alzheimer's disease. Brain Res 2013; 1519: 105-11.

Lammerding J, Fong LG, Ji JY, Reue K, Stewart CL, Young SG*, et al.* Lamins A and C but not lamin B1 regulate nuclear mechanics. J Biol Chem 2006; 281(35): 25768-80.

Lek M, Karczewski KJ, Minikel EV, Samocha KE, Banks E, Fennell T*, et al.* Analysis of protein-coding genetic variation in 60,706 humans. Nature 2016; 536(7616): 285-91.

Levin AA. Treating Disease at the RNA Level with Oligonucleotides. N Engl J Med 2019; 380(1): 57-70.

Liao H, Irvine AD, Macewen CJ, Weed KH, Porter L, Corden LD*, et al.* Development of allele-specific therapeutic siRNA in Meesmann epithelial corneal dystrophy. PLoS One 2011; 6(12): e28582.

Lin ST, Fu YH. miR-23 regulation of lamin B1 is crucial for oligodendrocyte development and myelination. Dis Model Mech 2009; 2(3-4): 178-88.

Liu J, Rolef Ben-Shahar T, Riemer D, Treinin M, Spann P, Weber K, *et al.* Essential roles for Caenorhabditis elegans lamin gene in nuclear organization, cell cycle progression, and spatial organization of nuclear pore complexes. Mol Biol Cell 2000; 11(11): 3937-47.

Loy RE, Lueck JD, Mostajo-Radji MA, Carrell EM, Dirksen RT. Allele-specific gene silencing in two mouse models of autosomal dominant skeletal myopathy. PLoS One 2012; 7(11): e49757.

Miller VM, Gouvion CM, Davidson BL, Paulson HL. Targeting Alzheimer's disease genes with RNA interference: an efficient strategy for silencing mutant alleles. Nucleic Acids Res 2004; 32(2): 661-8.

Miller VM, Xia H, Marrs GL, Gouvion CM, Lee G, Davidson BL, *et al.* Allele-specific silencing of dominant disease genes. Proc Natl Acad Sci U S A 2003; 100(12): 7195-200.

Mishra DK, Balekar N, Mishra PK. Nanoengineered strategies for siRNA delivery: from target assessment to cancer therapeutic efficacy. Drug Deliv Transl Res 2017; 7(2): 346-58.

Mistry A, Stolnik S, Illum L. Nanoparticles for direct nose-to-brain delivery of drugs. Int J Pharm 2009; 379(1): 146-57.

Nahhas NSR, P.; Vanderver, A.; Padiath, Q.S. Autosomal Dominant Leukodystrophy with Autonomic Disease. In: Adam MPA, H.H.; Pagon, R.A.; Wallace, S.E.; Bean, L.J.H.; Mefford, H.C.; Stephens, K.; Amemiya, A.; Ledbetter, N., editor. GeneReviews® [Internet]. Seattle (WA): University of Washington, Seattle; 2016.

Nguyen T, Menocal EM, Harborth J, Fruehauf JH. RNAi therapeutics: an update on delivery. Curr Opin Mol Ther 2008; 10(2): 158-67.

Nobrega C, Nascimento-Ferreira I, Onofre I, Albuquerque D, Deglon N, de Almeida LP. RNA interference mitigates motor and neuropathological deficits in a cerebellar mouse model of Machado-Joseph disease. PLoS One 2014; 9(8): e100086.

Nobrega C, Nascimento-Ferreira I, Onofre I, Albuquerque D, Hirai H, Deglon N, *et al.* Silencing mutant ataxin-3 rescues motor deficits and neuropathology in Machado-Joseph disease transgenic mice. PLoS One 2013; 8(1): e52396.

Osipovitch M, Asenjo Martinez A, Mariani JN, Cornwell A, Dhaliwal S, Zou L, *et al.* Human ESC-Derived Chimeric Mouse Models of Huntington's Disease Reveal Cell-Intrinsic Defects in Glial Progenitor Cell Differentiation. Cell stem cell 2019; 24(1): 107-22 e7.

Padiath QS, Saigoh K, Schiffmann R, Asahara H, Yamada T, Koeppen A, *et al.* Lamin B1 duplications cause autosomal dominant leukodystrophy. Nat Genet 2006; 38(10): 1114-23.

Prufert K, Vogel A, Krohne G. The lamin CxxM motif promotes nuclear membrane growth. J Cell Sci 2004; 117(Pt 25): 6105-16.

Quattrocolo G, Leombruni S, Vaula G, Bergui M, Riva A, Bradac GB, *et al.* Autosomal dominant late-onset leukoencephalopathy. Clinical report of a new Italian family. Eur Neurol 1997; 37(1): 53-61.

Rodriguez M, Kaushik A, Lapierre J, Dever SM, El-Hage N, Nair M. Electro-Magnetic Nano-Particle Bound Beclin1 siRNA Crosses the Blood-Brain Barrier to Attenuate the Inflammatory Effects of HIV-1 Infection in Vitro. J Neuroimmune Pharmacol 2017; 12(1): 120-32.

Rolyan H, Tyurina YY, Hernandez M, Amoscato AA, Sparvero LJ, Nmezi BC, *et al.* Defects of Lipid Synthesis Are Linked to the Age-Dependent Demyelination Caused by Lamin B1 Overexpression. J Neurosci 2015; 35(34): 12002-17.

Saraiva J, Nobre RJ, Pereira de Almeida L. Gene therapy for the CNS using AAVs: The impact of systemic delivery by AAV9. Journal of controlled release : official journal of the Controlled Release Society 2016; 241: 94-109.

Scholefield J, Greenberg LJ, Weinberg MS, Arbuthnot PB, Abdelgany A, Wood MJ. Design of RNAi hairpins for mutation-specific silencing of ataxin-7 and correction of a SCA7 phenotype. PLoS One 2009; 4(9): e7232.

Scholefield J, Watson L, Smith D, Greenberg J, Wood MJ. Allele-specific silencing of mutant Ataxin-7 in SCA7 patient-derived fibroblasts. Eur J Hum Genet 2014; 22(12): 1369-75.

Schwarz DS, Ding H, Kennington L, Moore JT, Schelter J, Burchard J, *et al.* Designing siRNA that distinguish between genes that differ by a single nucleotide. PLoS Genet 2006; 2(9): e140.

Shimi T, Butin-Israeli V, Adam SA, Hamanaka RB, Goldman AE, Lucas CA, *et al.* The role of nuclear lamin B1 in cell proliferation and senescence. Genes Dev 2011; 25(24): 2579-93.

Shrigley S, Pircs K, Barker RA, Parmar M, Drouin-Ouellet J. Simple Generation of a High Yield Culture of Induced Neurons from Human Adult Skin Fibroblasts. J Vis Exp 2018(132).

Smith FJ, Hickerson RP, Sayers JM, Reeves RE, Contag CH, Leake D, *et al.* Development of therapeutic siRNAs for pachyonychia congenita. The Journal of investigative dermatology 2008; 128(1): 50-8.

Takahashi M, Katagiri T, Furuya H, Hohjoh H. Disease-causing allele-specific silencing against the ALK2 mutants, R206H and G356D, in fibrodysplasia ossificans progressiva. Gene Ther 2012; 19(7): 781-5.

Takahashi M, Watanabe S, Murata M, Furuya H, Kanazawa I, Wada K, *et al.* Tailor-made RNAi knockdown against triplet repeat disease-causing alleles. Proc Natl Acad Sci U S A 2010; 107(50): 21731-6.

Tang CW, Maya-Mendoza A, Martin C, Zeng K, Chen S, Feret D, *et al.* The integrity of a lamin-B1-dependent nucleoskeleton is a fundamental determinant of RNA synthesis in human cells. J Cell Sci 2008; 121(Pt 7): 1014-24.

van den Boorn JG, Schlee M, Coch C, Hartmann G. SiRNA delivery with exosome nanoparticles. Nat Biotechnol 2011; 29(4): 325-6.

van Paassen BW, van der Kooi AJ, van Spaendonck-Zwarts KY, Verhamme C, Baas F, de Visser M. PMP22 related neuropathies: Charcot-Marie-Tooth disease type 1A and Hereditary Neuropathy with liability to Pressure Palsies. Orphanet J Rare Dis 2014; 9: 38.

Vergnes L, Peterfy M, Bergo MO, Young SG, Reue K. Lamin B1 is required for mouse development and nuclear integrity. Proc Natl Acad Sci U S A 2004; 101(28): 10428-33.

Wang S, Bates J, Li X, Schanz S, Chandler-Militello D, Levine C*, et al.* Human iPSC-derived oligodendrocyte progenitor cells can myelinate and rescue a mouse model of congenital hypomyelination. Cell stem cell 2013; 12(2): 252-64.

Whitehead KA, Langer R, Anderson DG. Knocking down barriers: advances in siRNA delivery. Nature reviews Drug discovery 2009; 8(2): 129-38.

Table 1. Genetic diseases associated with gene(s) duplication treatable by ASP-siRNA.

Disease	**OMIM**	**Locus**	**Target gene**
	Single gene disorders		
Parkinson disease	168600	4q21	*SNCA*
Adult-onset demyelinating leukodystrophy	169500	5q35	*LMNB1*
Charcot-Marie-Tooth type 1	118220	17p12	*PMP22*
Alzheimer disease	104300	21q21.3	*APP*
Pelizaeus-Merzbacher disease	312080	Xq22.2	*PLP1*
Rett syndrome	300260	Xq28	*MECP2*
	Genomic disorders		
Microduplication 7q11.23	609757	7q11.23	*ELN, GTF2I ?*
Spinocerebellar ataxia type 20	608687	11q12	*DAGLA?*
Microduplication 15q11-q13	608636	15q11.2-q13.1	*GABRA5?, GABRB3?, UBE3A*
Potocki-Lupski syndrome	610883	17p11.2	*RAI1*
Microduplication 17p13.3	613215	17p13.3	*LIS1, YWAHAE*
Microduplication 22q11.2	608363	22q11.2	*TXNRD2, COMT, ARVCF?*
Microduplication Xp11.22	300706	Xp11.22	*HUWE1I*

Note: question mark indicate proposed causative genes.

Figure 1

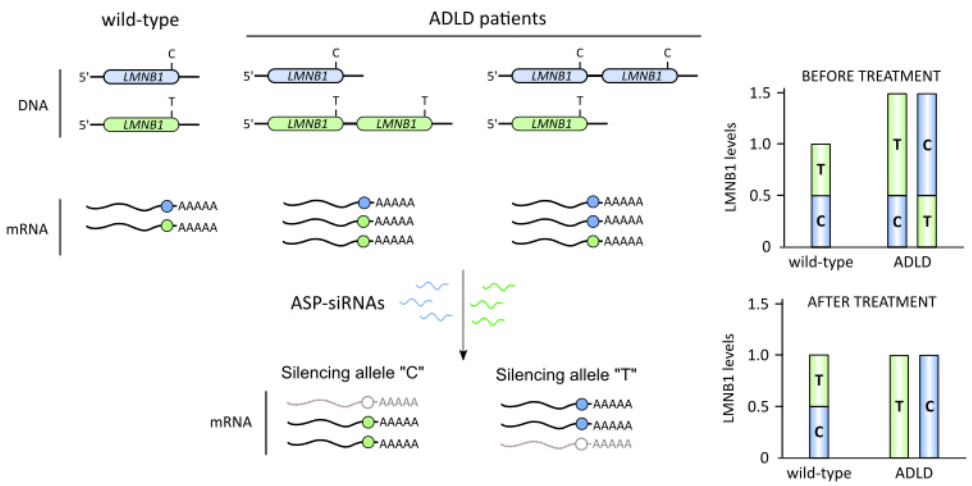

Fig. 1. Overview for the Allele Specific siRNA (ASP-siRNA) strategy. In Autosomal Dominant LeukoDystrophy (ADLD) patients, three copies of the lamin B1 (LMNB1) gene (rounded rectangles) are present due to a genomic duplication. We show some of the possible genomic conformations for the rs1051644 alleles that can have a "C" (light blue) or a "T" (green) polymorphic base. Below, analysis of the LMNB1 mRNA (curved line) from previous studies show an equal expression of the three alleles (Giorgio et al., 2013). Silencing of the non-duplicated allele by ASP-siRNA is the best strategy to reduce the amount of LMNB1 without excessively downregulating the gene. The histograms show that in an optimal situation, following ASP-siRNA treatment, the amount of LMNB1 is reduced to the level of wild-type due to the specific knockdown of one allele.

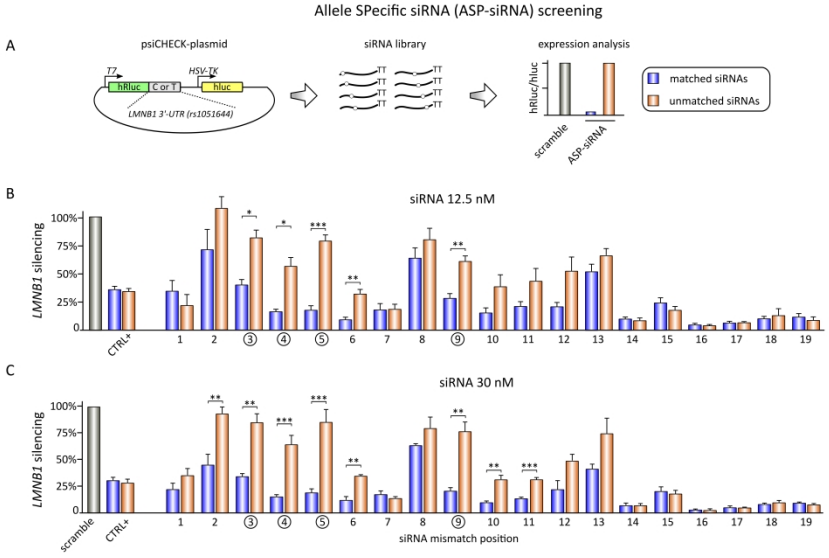

Fig. 2. Allele Specific siRNA screening. In panel A, the rationale used to identify efficient and allele-specific siRNA. Using a psiCHECK dual luciferase vector, we cloned part of the 3'-UTR of LMNB1 downstream to the hRluc gene (green rectangle) used as reference. The hluc gene (Renilla, yellow rectangle) in the plasmid is used to normalize the transfection efficiency (T7 and HVV-TK indicate promoter types). Two vectors were generated, one with the "T" and one with the "C" allele at rs1051644. The reporter vector was challenged with each of 19 siRNA containing the rs1051644 "C" or "T" allele in one of the 19 possible positions (see Suppl. table 2 for details) at two different concentrations (12.5 nM, panel B; 30 nM, panel C). A scramble siRNA and a siRNA against hRluc were used as negative and positive controls, respectively. Ideally, the best siRNA should completely abrogate the matched allele, leaving the unmatched allele unchanged (panel A, histograms). Results of this screening are reported in panels B and C. Numbers on the X-axis indicate the position of the mismatch on the siRNA. CTRL+ indicate a non-allele specific LMNB1 siRNA. Statistical significant differences (asterisks) between matched (blue) and unmatched (orange) siRNAs are reported ($p<0.05$: *; $p<0.01$: **; $p<0.001$: ***; two-tailed, Mann-Whitney). The most efficient and allele-specific siRNAs are circled.

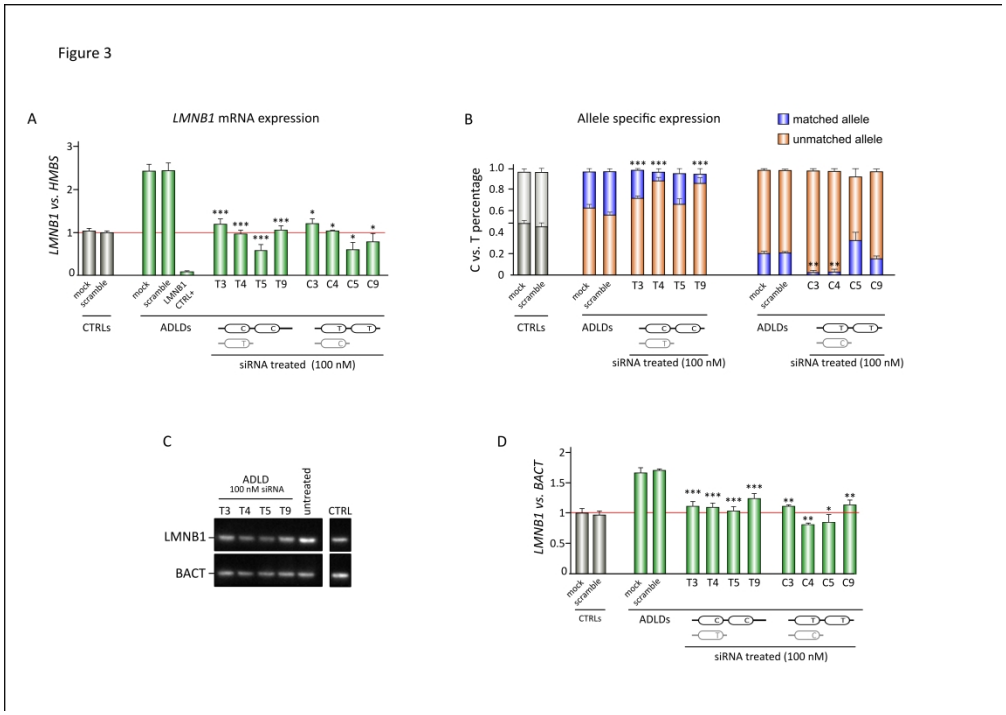

Fig. 3. Primary readouts of ASP-siRNA efficacy. ADLD fibroblasts with the "C" allele on the duplicated LMNB1 copy were treated with 100 nM ASP-siRNAs against the "T" allele of rs1051644 and vice versa for 48 hours; mock = untreated cells. Four different ADLD cell lines and three age-matched controls were tested. At least three independent technical replicas were performed. In panel A, evaluation of total LMNB1 mRNA levels by quantitive RT-PCR (LMNB1 vs HMBS). Fold change and SEM (bars) are reported. Statistical significance is given comparing ADLD vs scramble ($p<0.05$: *; $p<0.01$: **; $p<0.001$: ***; two-tailed, Mann-Whitney). In panel B, evaluation of allele-specific expression using primer extension assay (allele C versus allele T, percentage). Mean ± SEM (bars) are reported. Statistical significant values were evaluated comparing ADLD vs scramble ($p<0.01$: **; $p<0.001$: ***; two-tailed, Mann-Whitney). In panels C and D, evaluation of total LMNB1 protein by western blot (LMNB1 vs β-actin). Immunostaining with anti-LMNB1 and anti-β-actin antibodies are shown as exemplification of the analysis in panel C. Fold-change densitometric data and SEM (bars) are shown in panel D. Statistical significant differences (asterisks) is reported for ADLDs vs. scramble ($p<0.05$: *; $p<0.01$: **; $p<0.001$: ***; two-tailed, Mann-Whitney). D- Schematic drawing showing the genomic structure of ADLD patients used in the experiments in reference to rs1051644.

Figure 4

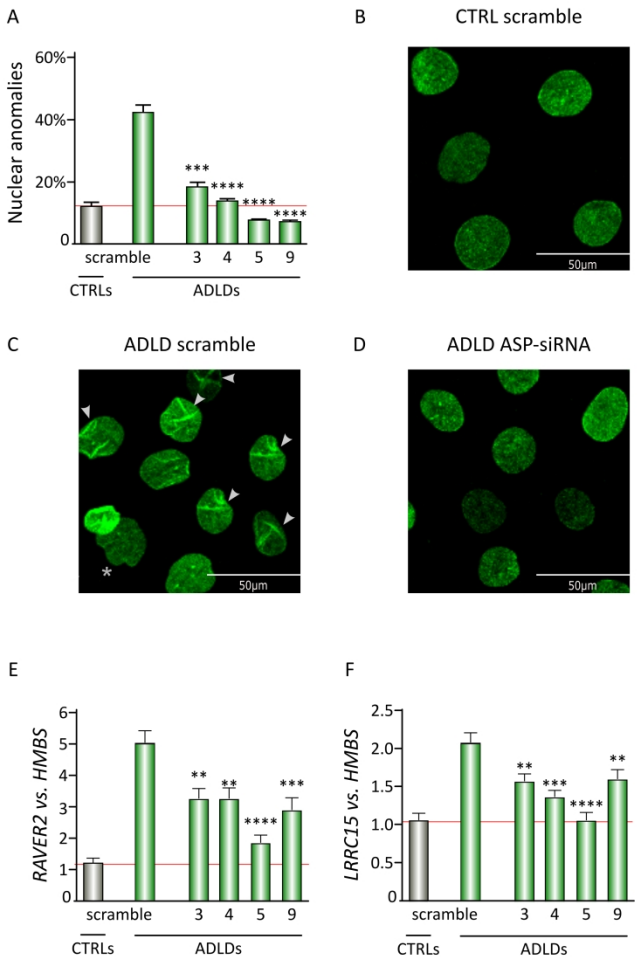

Fig. 4. Secondary readouts of ASP-siRNA efficacy. ADLD fibroblasts with the "C" allele on the duplicated LMNB1 copy were treated with 100 mM ASP-siRNAs against the "T" allele of the SNP and vice versa for 120 hours. Four different ADLD cell lines and three age-matched controls were tested. At least three independent experiments were performed. Nuclear shape anomalies were evaluated by fluorescent microscopy after LMNB1 staining. A total of 5,391 nuclei were evaluated in blind. Fold-change and SEM (bars) are shown in panel A. Statistical significant values show differences between ADLD and scramble ($p<0.001$: ***; $p<0.0001$: ****; two-tailed, Mann-Whitney). Nuclei from a control line treated with scramble siRNA (CTRL scramble, panel B) and an ADLD line treated with scramble siRNA (ADLD scramble, panel C) or with ASP-siRNAs (ADLD ASP-siRNA, panel D) are shown as exemplification of the analysis. Blebs (asterisk) and invaginations (arrow heads) are highlighted. E-F. Histograms show quantitative real-time PCR results for RAVER2 mRNA levels (panel E; RAVER2 vs HMBS) and LRRC15 (panel F; LRRC15 vs HMBS). Fold change and SEM (bars) are reported. Statistical significant differences (asterisks) is given for ADLDs vs. scramble ($p<0.02$: **; $p<0.001$: ***; $p<0.0001$: ****; two-tailed, Mann-Whitney).

Figure 5

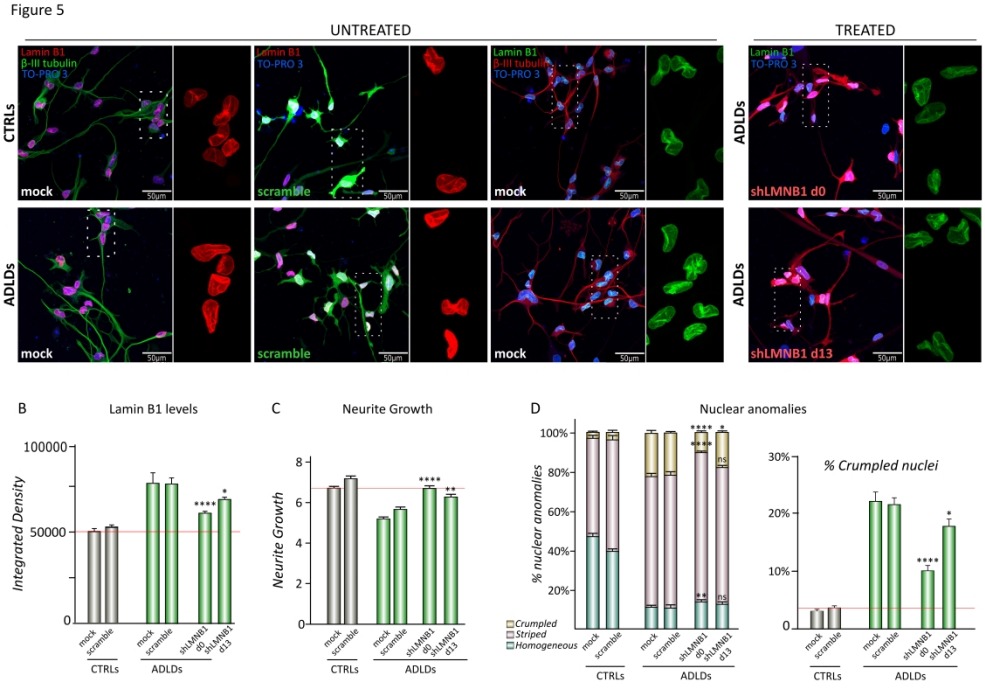

Fig. 5. Validation of ASP-RNAi in reprogrammed neurons. Panel A shows neurons directly reprogrammed from fibroblasts of ADLD patients (ADLDs) or healthy subjects (CTRLs), stained for β-III tubulin. Neurons were cultured with no treatments (mock), or transduced with either scramble lentiviral particles (scramble) or with shLMNB1 viruses at two different time points, reprogramming day 0 or day 13 (shLMNB1 d0; shLMNB1 d13). For each panel a 2 fold magnified inset is shown. Note that labelling for Lamin B1 protein is presented in green or red, in accordance with the corresponding fluorescent reporter encoded by the infecting viral particles. Panels B, C and D show, respectively, quantifications of Lamin B1 protein levels, neurite growth and nuclear anomalies in cells untreated (mock), infected with LV-scramble shRNA (scramble) or with the ASP-vector at d0 (shLMNB1 d0) or d13 (shLMNB1 d13). Examples of nuclei corresponding to the categories represented in Panel D are shown in Suppl. Fig. 1 (Panel E). Statistically significant differences (asterisks) are shown for comparisons between ADLDs shLMNB1 vs. ADLD scramble (panel B: Mann-Whitney t-test ;****, p< 0.0001; *, p= 0.0316; panel C: Mann-Whitney t-test; ****, p< 0.0001; **, p= 0.0030; panel D: Mann-Whitney t-test; d0, crumpled nuclei, ****, p< 0.0001; d0 striped nuclei, **, p= 0.0046; d13 crumpled nuclei, *, p= 0.0100; ns, p> 0.05). Details of statistical analysis for all comparisons are reported in Suppl. Table 8. Error bars: SEM. Staining: Lamin B1 (green or red), β-III tubulin (green or red), LV-scramble (green), ASP-vector (red), cell nuclei/TO-PRO-3 (blue). Scale bars are shown.

Figure 6

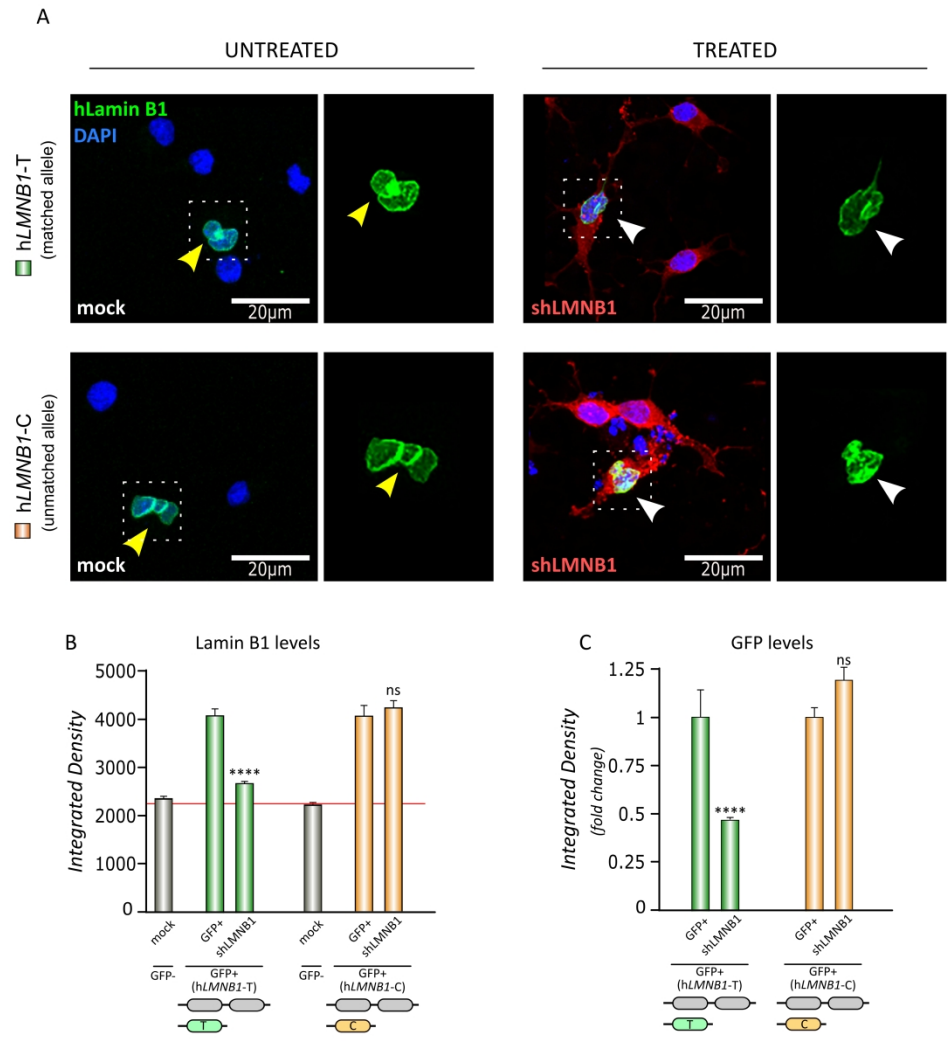

Fig. 6. Validation of ASP-RNAi in OPCs overexpressing hLMNB1. Panel A shows OPCs transfected to overexpress the 'T' (hLMNB1-T; up) or the "C" (hLMNB1-C; down) allele of the GFP-tagged human LMNB1 (yellow arrows). The human GFP-tagged Lamin B1 protein (green) localizes to the cell nuclei (DAPI staining, blue), as expected. Cells were cultured with no treatments (mock; untreated: left) or transduced with the ASP-vector (shLMNB1; treated: right). White arrows indicate effectively transfected (GFP+, green) and transduced (red) cells. For each panel a 2× magnified inset displaying GFP-tagged Lamin B1 is shown. OPCs, oligodendrocyte progenitor cells. Staining: hLamin B1-GFP protein (green), cells transduced with LV-shLMNB1 (shLMNB1, red), nuclei, DAPI (blue). Scale bars are shown. Panel B shows quantifications of total Lamin B1 protein levels obtained by analyses of human and mouse Lamin B1 immunostaining in cells untreated (GFP-; mock), transfected with the GFP-tagged human Lamin B1 "T" allele (GFP+ hLMNB1-T) or the GFP-tagged human Lamin B1 "C" allele (GFP+ hLMNB1-C), or transfected and treated with the LV-shLMNB1 (shLMNB1). Panel C shows quantifications of human Lamin B1 protein levels based on tagged GFP fluorescence in cells transfected with the GFP-tagged human Lamin B1 "T" allele (GFP+ hLMNB1-T) or the GFP-tagged human Lamin B1 "C" allele (GFP+ hLMNB1-C) or transfected (GFP+) and infected with the LV-shLMNB1 (shLMNB1). Statistically significant differences are shown for GFP+ shLMNB1 vs. GFP+ or GFP-

cells (Mann-Whitney t-test ;****, $p < 0.0001$; ns, $p > 0.05$).

Supplementary materials and methods.

Dual-reporter plasmids for siRNAs' screening. The 3'-UTR of the *LMNB1* gene (chr5:126,171,957-126,172,712; hg19) was PCR-amplified from a genomic DNA heterozygous for the rs1051644 SNP under standard conditions. Forward and reverse primers contained a 5'-*XhoI* and a 5'-*NotI* restriction site respectively (Suppl. table 1). PCR products were gel-purified with the GenElute Gel Extraction kit (Sigma-Aldrich, Darmstadt, Germany), and inserted into the pGEM-T plasmid using the pGEM-T easy vector system I (Promega, Madison, WI). Plasmids were transformed using JM109 competent cells (Promega), harvested and extracted using the PureYield Plasmid Miniprep System (Promega). Plasmids containing the "C" or the "T" rs1051644 allele were selected by Sanger sequencing. Subsequently, a pGEM-T plasmid for each allele was double-digested with *XhoI* and *NotI*. The insert was gel-purified and ligated into a psiCHECK^{TM}-2 system (Promega). After clone harvesting, we selected one psiCHEK-LMNB1-3'UTR-C and one psiCHEK-LMNB1-3'UTR-T clone whose insert was completely Sanger sequenced. In these expression vectors, the 3'-UTR insert carrying the "C" or "T" allele is fused to the *Renilla Luciferase* (*hRluc*) gene after the translational stop codon. A *Firefly Luciferase* (*hluc+*) gene in the same vector is used as an internal standard to normalize *Renilla* activity. Plasmids were finally re-transformed into JM109 competent cells (Promega), harvested and extracted using the PureYield Plasmid Midiprep System (Promega) for transfection.

Human *LMNB1*- green fluorescent protein (*AcGFP*) tagged expression plasmid. In brief, cDNAs encoding full-length human *LMNB1* (hLMNB1; C-allele and T-allele for the SNP rs1051644) have been amplified and sub-cloned into the CAGP-AcGFP1 plasmid (Vector Builder, Santa Clara, CA, USA), generating the CAGP-AcGFP1-hLMNB1 vector. The vector produced an AcGFP1-tagged LMNB1 protein which showed nuclear localization and physiological turnover (data not shown).

Direct reprogramming plasmid for fibroblast-to-neuron differentiation. To improve the fibroblast-to-neuron conversion efficiency, and the reproducibility of the method, we generated the pABR vector by combining four reprogramming elements in a single construct. The pAB plasmid (pCCLsin.cPPT.hPGK.BRN2-hPGK Ascl1 WPRE) expressing m*Ascl1* and m*Brn2* was used as

destination plasmid to insert the two short hairpin RNAs for *REST* knock-down (pREST_sh1, pREST_sh2) (kindly donated by Malin Parmar, University of Lund, Sweden, details available upon request; see Suppl. Table 1). Next, the assembled pABR vector was transformed and expanded into DH5α competent cells (New England Biolabs, Ipswich, MA, USA) and used to generate the corresponding lentivirus (LV-ABR). An identical construct was independently generated and published by Malin Parmar's group (Drouin-Ouellet *et al.*, 2017).

To evaluate the relative expression of each element assembled in the pABR vector, the fibroblast line MGM1800E was infected with the same dose of lentivirus carrying the assembled vector (pABR), each of the previous vectors (pAB, pREST_sh1, pREST_sh2) and the combination of the three vectors (AB+sh1+sh2). The infected cells were collected and the RNA analyzed by real time qPCR (Suppl. Table 1). The gene expression analysis confirmed the functionality of the LV-ABR in terms of expression of mAscl1 and mBrn2 transgenes and of downregulation of endogenous REST transcript (Suppl. Fig. 1A-C).

Supplementary figures and legends.

Suppl. Fig. 1. Direct reprogramming of human fibroblasts into neurons and identification of disease-specific cellular phenotypes.

Panels A-C shows real-time PCR analyses of the three genes involved in the neuronal conversion of the fibroblasts. Histograms represent expression levels of murine *Ascl1* mRNA levels (panel A; m*AScol1* vs *18S*), murine *Brn2* mRNA levels (panel B; *mBrn2* vs *18S*) and human *REST* mRNA levels (panel C; *hREST* vs *18S*). Fold change and SEM (bars) are reported. Control: non infected cells; AB: cells infected with pCCLsin.cPPT.hPGK.BRN2-hPGK Ascl1 WPRE; sh1: cells infected with 3282 pLKO.1-puro_REST_sh_seq1 WPR; sh2: cells infected with 3282 pLKO.1-puro_REST_sh_seq2 WPRE; AB+sh1+sh2: cells infected with a combination of the previous vectors. ABR: cells infected with the assembled vector. The gene expression analysis confirms the functionality of the LV-ABR in terms of expression of mAscl1 and mBrn2 transgenes and of downregulation of endogenous REST transcript. Panel D shows efficiently reprogrammed neurons, identified by anti- β-III tubulin staining and obtained from both healthy donors (CTRLs) and patients (ADLDs) (day 20 after infection with reprogramming vectors). About 60% of cells (58% CTRLs; 64% ADLDs) have been effectively reprogrammed into neurons. Panel E shows analyses on ADLD-derived neurons. Evaluation of Lamin B1 protein levels by integrated density analysis of anti-LMNB1 staining confirms overexpression in patients' derive cells (Mann-Whitney t-test; ****, $p<0.0001$). Evaluation of neurites indicates reduced neurite outgrowth in ADLD cells to healthy subjects-derived neurons (Mann-Whitney t-test; ***, $p< 0.0001$). Evaluation of nuclear anomalies. At 20 days after differentiation, ADLD cells display a higher frequency of striped or crumpled nuclei compared to healthy subjects-derived neurons. (Mann-Whitney t-test;**, $p=0.0034$). Error bars: SEM. Staining: Lamin B1 (green), β-III tubulin (red). Scale bars are shown.

Suppl. Fig. 2. Rat OPC cultures overexpressing human GFP-tagged Lamin B1 (hLamin B1). Panel A shows NG2 positive rat OPCs transfected in order to overexpress the 'T' or the "C" allele of

the GFP-tagged human LMNB1 (hLamin B1-GFP; white arrows). The transfection efficiency obtained was about 3 %. The human GFP-tagged Lamin B1 protein (green) localizes to the cell nuclei (DAPI staining, blue), as expected. Nuclear fragmentation of a transfected cell is highlighted in the inset (I). Panel B shows transfected OPCs (yellow arrows) which show a more intense immunostaining for Lamin B1 compared to non-transfected cells (white arrows), as highlighted in the insets (I,II). A 3 fold magnified insets are shown. Panel C shows the analysis of total Lamin B1 levels (human and mouse, as detected by immunostaining) in transfected GFP+ vs. non-transfected GFP- OPCs (Mann-Whitney t-test; *, p=0.0177). Panel D shows that, upon Lamin B1 overexpression, a specific type of nuclear anomalies is observed. Namely, multiple nuclear stripes (III) and a unique nuclear constriction pattern (red arrows, IV) suggestive of ongoing nuclear fragmentation appear in about 5% of transfected cells (as measured over 1119 cells), while non-transfected cells and cells transfected with the GFP-empty vector (not shown) display a homogeneous hLamin B1-GFP nuclear distribution with occasional Lamin B1 condensed to form individual stripes (I, II). OPCs, oligodendrocyte progenitor cells. Staining: hLamin B1-GFP (green), total Lamin B1 protein (Lamin B1, white), membrane proteoglycan NG2 protein (red), DAPI (blue). Scale bars are shown.

Supplementary Figure 1

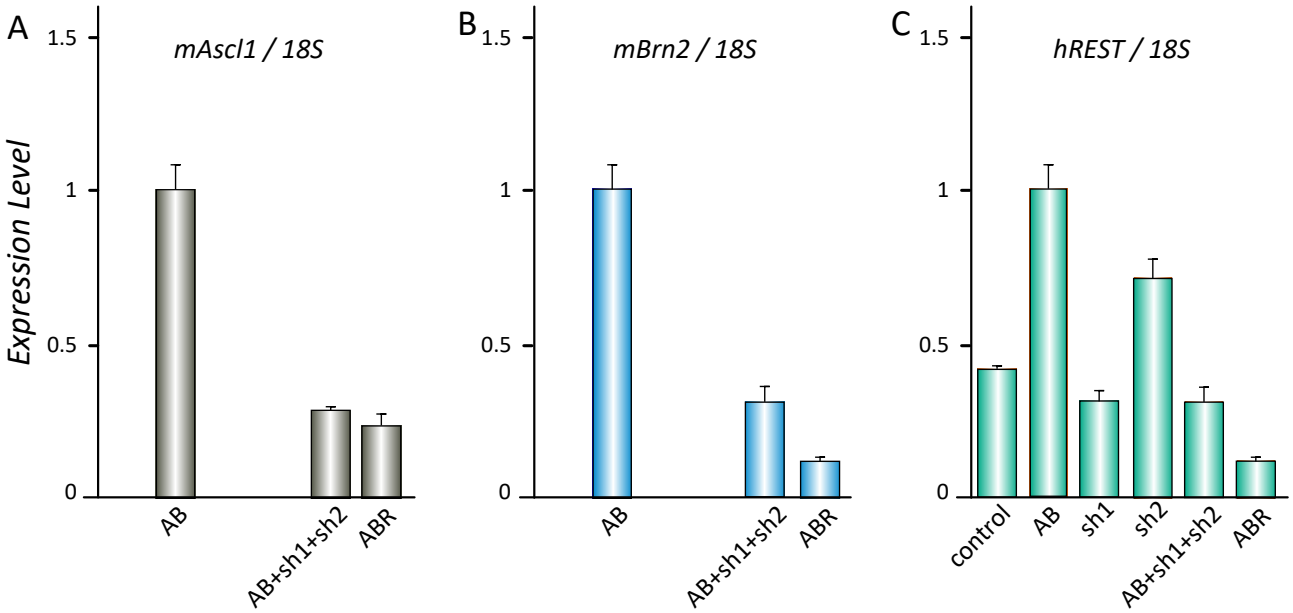

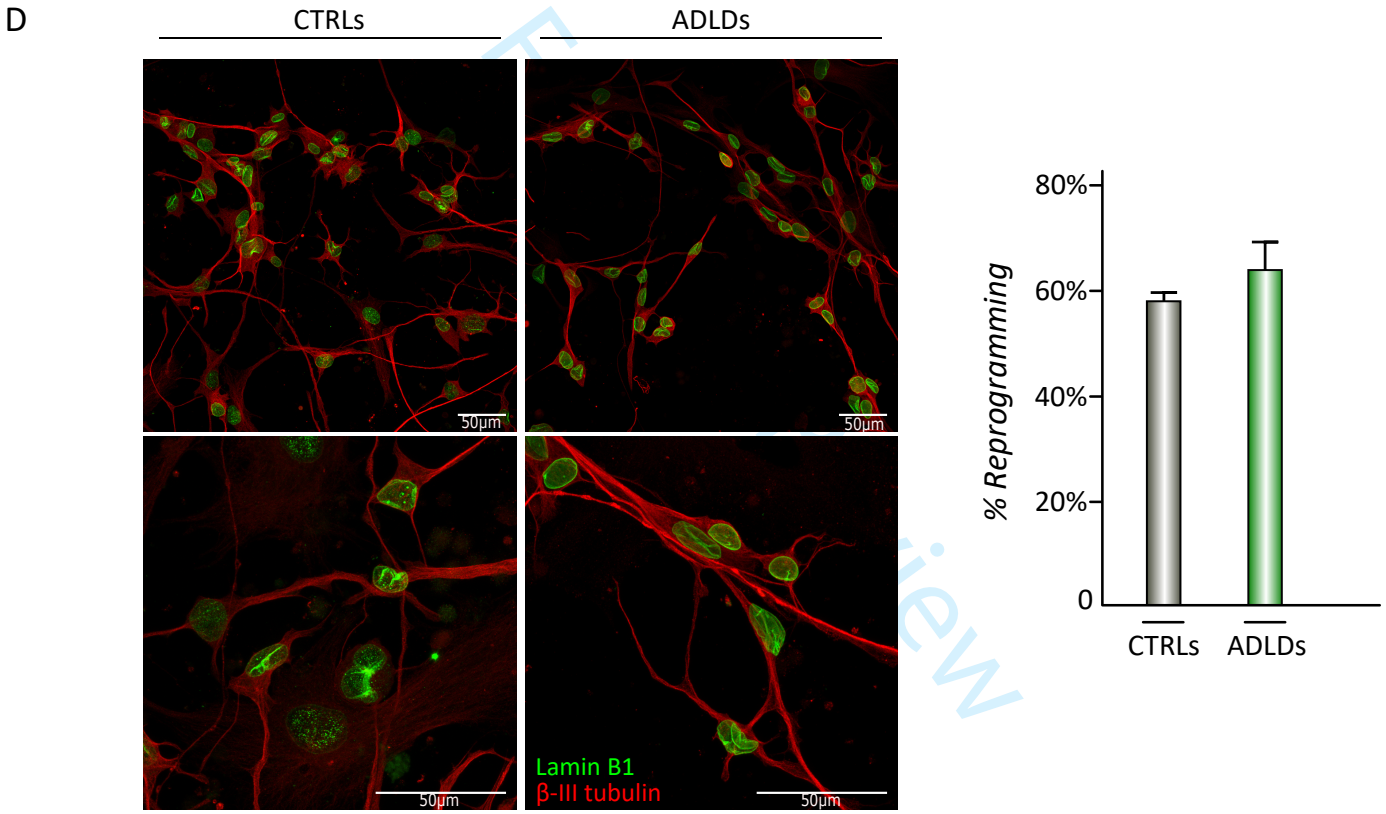

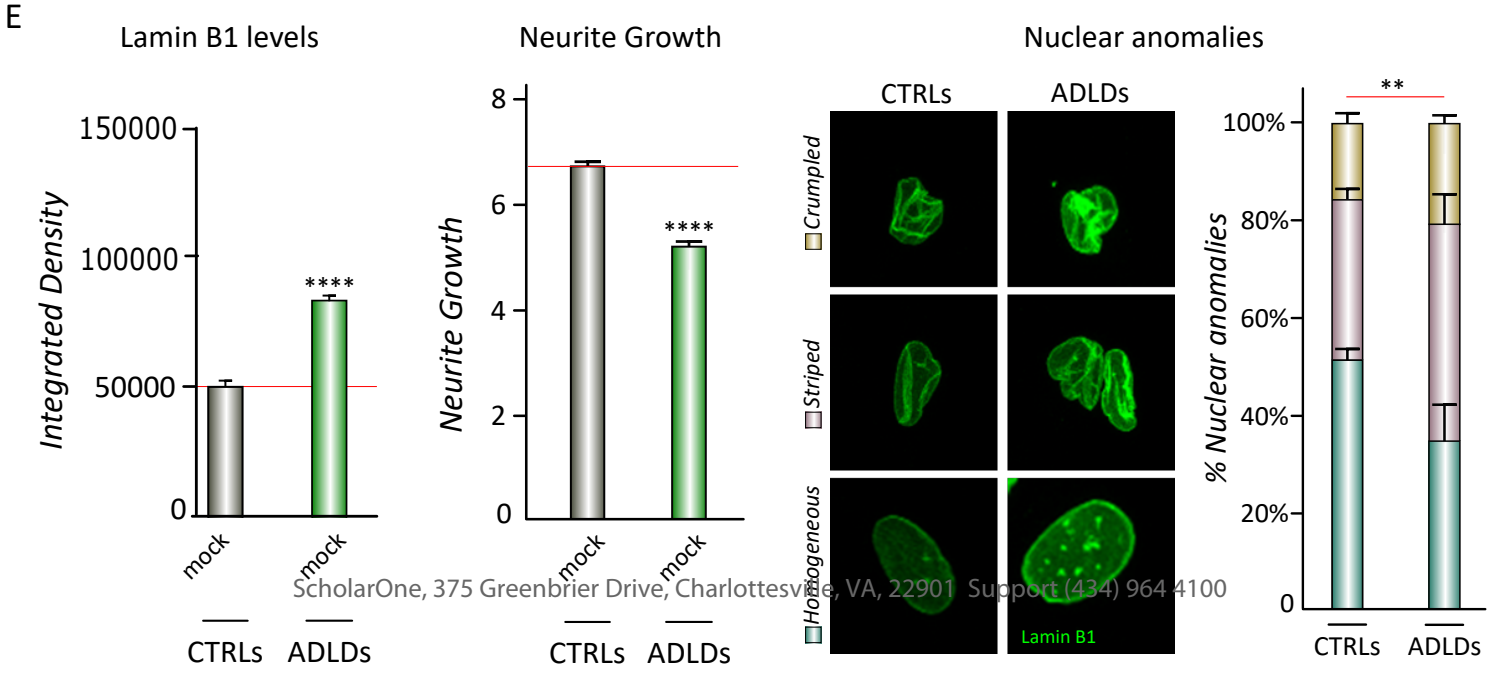

Supplementary Figure 2